Heliyon 10 (2024) e31655

Contents lists available at ScienceDirect

Heliyon

journal homepage: www.cell.com/heliyon

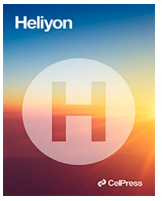

Research article

Multi-objective optimization and 4E (energy, exergy, economy, environmental impact) analysis of a triple cascade refrigeration system

Imrul Kayes , Raditun E. Ratul , Abyaz Abid , Fawaz Bukht Majmader , Yasin Khan , M Monjurul Ehsan *

Department of Mechanical and Production Engineering (MPE), Islamic University of Technology (IUT), Board Bazar, Gazipur-1704, Bangladesh

A R T I C L E I N F O

Keywords:
Cascade refrigeration
Economic analysis
Environmental impact
Multi-objective optimization
Hydrocarbon refrigerants
Box-behnken method

A B S T R A C T

The post-pandemic energy crisis and ever-increasing environmental degradation necessitate researchers to scrutinize refrigeration systems, major contributors to these issues, for minimal environmental impact and maximum performance. Thus, this study aims to comprehensively examine a triple cascade refrigeration system (TCRS) equipped with hydrocarbon refrigerants (1-butene/Heptane/m-Xylene). This system is specifically designed for ultra-low temperature applications, including vaccine storage, quick-freezing, frozen food preservation, cryogenic processes, and gas liquefaction. The investigation integrates conventional thermodynamic analysis with economic and environmental impact assessments, and finally multi-objective optimization (MOO) to ascertain optimal operating conditions for the system. The effect of (1) evaporator temperature, T_{evap} (2) condenser temperature, T_{cond} (3) Lower Temperature Circuit (LTC) condenser temperature, T_{LTC} (4) Mid Temperature Circuit (MTC) condenser temperature, T_{MTC} and (5) Cascade Condenser temperature difference, ΔT on three objective functions (COP, exergy efficiency, and overall plant cost) have been investigated employing a parametric analysis. Subsequently, quadratic equations for these objective functions are generated using the Box-Behnken method, and MOO utilizing the Genetic algorithm has been performed to maximize COP and exergy efficiency while minimizing the overall cost rate. The decision-making techniques TOPSIS and LINMAP are used to retrieve a unique solution from the Pareto Front, and the system performance has been assessed at the optimal point. The optimization result demonstrates that for the 10-kW capacity TCRS, COP, exergy efficiency, and total plant cost are 0.71, 0.51, and 38262.05 $/year respectively, at optimum condition ($T_{evap} = -101.023\ ^{\circ}C$, $T_{cond} = 36.545\ ^{\circ}C$, $T_{LTC} = -69.047\ ^{\circ}C$ and $T_{MTC} = -34.651\ ^{\circ}C$). Exergy analysis identifies HTC compressor (19.3 %) and throttle valve (15.5 %) as key contributors to total exergy destruction, while economic analysis underscores capital and maintenance costs (72 %) as the primary contributors to the overall cost, with evaporator (43 %) and condenser (20 %) accounting for 63 % of this cost.

1. Introduction

Energy scarcity and environmental degradation have become critical issues in recent times. The rising need for refrigeration in a

* Corresponding author.
E-mail address: ehsan@iut-dhaka.edu (M.M. Ehsan).

https://doi.org/10.1016/j.heliyon.2024.e31655
Received 29 September 2023; Received in revised form 5 January 2024; Accepted 20 May 2024
Available online 23 May 2024

Nomenclature

Abbreviation

BBD	Box-Behnken design
CHX	Cascade heat exchanger
COP	Coefficient of performance
CRF	Capital recovery factor
CRS	Cascade refrigeration system
C & M	Capital and maintenance
GWP	Global warming potential
HTC	High temperature circuit
HTCC	HTC compressor
LMTD	Logarithmic mean temperature difference
LTC	Lower temperature circuit
LTCC	LTC compressor
MAE	Mean absolute error
MAPE	Mean absolute percentage error
MTC	Mid temperature circuit
MTCC	MTC compressor
ODP	Ozone depletion potential
PH	Physical
RMSE	Root mean squared error
RSM	Response surface methodology
TCRS	Triple cascade refrigeration system

Greek letter

η	Exergy efficiency (%)
μ	Emission factor
α	Electricity cost
φ	Maintenance factor

Symbols

$\dot{C}$	Cost rate ($/year)
e	Specific exergy (kJ/kg)
$\dot{E}$	Exergy rate (kW)
h	Enthalpy (kJ kg^{-1})
$\dot{m}$	Mass flow rate (kg s^{-1})
P	Pressure (kPa)
$\dot{Q}$	Heat transfer rate (kW)
s	Entropy (kJ kg^{-1} K^{-1})
T	Temperature ($^{\circ}C$)
$\dot{W}$	Work input rate (kW)

Subscripts

1,2 …	State points
cond	Condenser
D	Exergy destruction
e	Electrical
evap	Evaporator
F	Exergy of fuel
i	Isentropic
m	Mechanical
P	Exergy of product
TV	Throttle valve

variety of areas such as the food and beverage industry, pharmaceuticals and healthcare, chemical and industrial processes, retail and commercial, agriculture and Horticulture, research, and laboratories makes this a significant contributor to these critical issues, as refrigeration and air conditioning sector consumes 20 % of global energy demand, according to a recent report by IIR [1] and most commonly employed refrigerants (CFCs, HCFCs, and HFCs) have been accountable for severe consequences of the environment such as

ozone depletion and temperature rise [2,3]. Several laws, such as the Montreal Protocol of 1987, the Kyoto Protocol of 1997, and the Kigali Amendment (2016), have been enacted by world leaders to reduce the use of synthetic refrigerants, which are considered greenhouse gases. Thus, refrigeration systems employing environment-friendly refrigerants that pose minimal plant cost and performance compromise have become one of the most crucial goals for researchers all around the world to attain [4].

The requirement for refrigeration with extremely low temperatures (ranging from $-50\,^{\circ}C$ to $-180\,^{\circ}C$) is escalating as a result of the rapid expansion of global civilization, particularly for applications involving quick-freezing [5], preservation of medical supplies [6], and frozen food preservation to retain quality and inhibit the growth of pathogenic bacteria [7], in an assortment of industrial processes, including the natural gas [8,9] and the petroleum gas [10] liquefication, military and national defense equipment [8], steel alloy treatment processes [11], vaccines and other medicines preservation for viruses like Covid-19 which needs about $-70\,^{\circ}C$ [12], cryogenic processes which are below $-100\,^{\circ}C$ [13,14], and other applications which require exceedingly low temperatures (freeze drying and chemical industries [15]). It's not viable to employ a refrigeration system that consists of just one stage of vapor compression due to thermodynamic or economic considerations, as a large temperature gap between the evaporator and the condenser demands high pressure ratio, which results in poor volumetric compressor efficiency, compressor's wear & tear, increase in compressor power, decrease in cooling effect and ultimately poor 1st law efficiency [16–18]. Furthermore, this large temperature gap results in a decreased evaporator pressure (which makes the system vulnerable to air leakage) and a rise in condenser pressure as well as suction volume (which demand robust pipe designs and fitting that ultimately results in a higher plant cost rate) [19]. Implementing cascaded refrigeration in which the condenser of a Vapor Compression Refrigeration (VCR) unit is thermally coupled with the evaporator of a second unit could address the challenges mentioned above [10].

1.1. Study on double stage VCR systems

The Double Cascade Refrigeration System (CRS) has been investigated extensively as an efficient system to be utilized at low temperatures. Various refrigerants are used in double cascade refrigeration systems, such as CO_2–NH_3 [19–21], R717, R744, R1270, R134a [22,23], transcritical CO2–C3H8 [24], R11 [25], Mixture of different refrigerants, etc. [20]. Sun et al. [21] did a simulation on double CRS employing the refrigerant pairs R41/R23 in LTC and R404A in Higher Temperature Circuit (HTC) and concluded that R41-R404A gives superior performance. Saleh et al. [22] used Aspen HYSYS to optimize the process of employing several environmentally friendly refrigerants inside the system, with a particular emphasis on minimizing compressor power. Double stage VCR system has been analyzed via simulation by many researchers including Bhattacharyya and Sarkar [23], Getu and Bansal [24], Aktemur et al. [25], Kilicarslan and Hosoz [26], Llopis et al. [27], Soni et al. [28].

1.1.1. Experimental works and practical applications of double stage VCR systems

Although the practical application of the double-stage VCR system remains limited, it exhibits potential across various sectors. It has been applied in supermarkets by several researchers, including Eggen and Aflekt [29], Pearson and Cable [30], Van Riessen [31], Sawalha et al. [32], Da Silva et al. [33]. It has been practically employed and analyzed in vaccine storage task as well by Liu et al. [34]. Some notable contributions to the experimental analysis include the works of S. Cabello et al. [35], Bingming et al. [36], Dopazo and Ferna'ndez-Seara [37], Sanz-Kock et al. [38], Wang et al. [39] and Jeon [40]However, for sectors that require ultra-low temperatures, maintaining the corresponding high-pressure ratio is not feasible with a double cascade system. Cascade refrigeration systems with three stages, a relatively recent innovation in this field, could be a cost-effective solution to this problem [41].

1.2. Study on triple cascade VCR systems

A Triple Cascade Refrigeration (TCR) system is comprised of three shared single-stage refrigeration cycles called LTC, MTC, and HTC. The process of liquefaction of LNG was researched by Najibullah et al. [42], who studied the usage of three stage refrigeration for Propane precooling. This work demonstrates the system's enhanced efficiency as an outcome of achieving optimum operating conditions by simulation. Yoon et al. [43] proposed a TCR in the liquefication of natural gas. A mixture of methane, propane, and ethylene was used as a refrigerant in another system. The efficiency was increased significantly compared to a single-stage system and increased by 25 % compared to an optimized TCR system using the later refrigerant mixture. Johnson et al. [44] developed a TCRS for cryogenic applications. The system employed methane, propylene, and ethylene to achieve $-158\,^{\circ}C$ evaporator temperature and it was then utilized for extracting the methane and carbon monoxide in a cryogenic column for distillation. Qin et al. [45] proposed a triple stage auto cascade refrigeration system employing refrigerants R1234yf/R23/R14 and they were able to achieve a 26 % efficiency of exergy and a COP of 0.614. A thorough thermodynamic investigation of a TCRS to be utilized at very low temperatures was conducted by Faruque et al. [41] at an evaporator temperature of 100 °C. These results demonstrate the potential for hydrocarbon refrigerants to maintain high thermodynamic efficiency in applications involving exceedingly low temperatures. Sun et al. [10] proposed a TCR utilizing refrigerants of low GWP, and thermodynamic analysis on this system determined that R1150, R152a, R41, R170, R717, and R161 are suitable alternatives in various temperature cycles, providing a theoretical basis for refrigerant selection and replacement in TCRS with environmental protection in mind.

1.2.1. Experimental works related to TCRS

To the best of the authors' knowledge, the application of TCRS has been predominantly confined to simulation, with no corresponding experimental investigations conducted thus far. Nevertheless, considering the successful implementation of the double cascade VCR system in various applications operating on a similar principle, it is evident that TCRS harbors the potential for effective

deployment in real-life ultra-low temperature applications.

1.3. Study on economic analysis

The main objective of the above articles is a thermodynamic investigation aimed at either maximizing COP or minimizing exergy destruction. While this approach enhances efficiency, it has the potential to lead to a significant escalation in the cost. Because of rising energy prices, increasing worldwide demand for energy, and rising environmental concerns, more effective, economical, and eco-friendly methods of energy usage are in great demand. So, when analyzing a refrigeration plant, it is crucial to consider economic factors as well [46]. The thermo-economic technique is an appropriate strategy for analyzing systems from both the economic and thermodynamic aspects. By incorporating elements of economic and exergy analysis, this method ensures improved performance at the lowest possible cost [47]. Thermo-economic modelling of frost-free freezers and subsequent optimization was conducted by Mitishita et al. [48]. Rezayan and Behbahaninia [19] also conducted investigations on cascade refrigeration systems with CO_2/NH_3 using a thermo-economic approach and obtained optimized results.

1.4. Study on multi objective optimization

Multi-objective optimization (MOO) is a useful tool for solving problems with several competing goals. It involves identifying a collection of solutions called the Pareto front. These solutions offer an optimal compromise between distinct objectives without being overshadowed by any other alternative concerning all the goals simultaneously [49,50]. It has diverse applications across areas like finance, engineering, or decision-making processes where trade-offs between various criteria call for consideration [51,52]. This technique empowers its users to evaluate different scenarios and make well-informed choices based on their constraints and preferences. Gebreslassie et al. [53] investigated a sustainable and single-effect water/LiBR absorption cycle using MOO. For an ice thermal energy storage (ITES) system, Sanaye and Shirazi [54] used MOO approaches. Similarly, for applications in air conditioning, Navidbakhsh and Shirazi [55] used the MOO strategy to develop a PCM-incorporated ITES system. The studies that are closely related to this work (application of MOO on CRS) are listed in Table 1.

1.5. Research scope and problem statement

Following the devastating COVID-19 pandemic, TCRS' demand has skyrocketed due to its use in ultra-low temperature applications, particularly in vaccine supply chains and the pharmaceutical industry. Thus, a comprehensive examination of this system is critically important [34]. The comprehensive literature review indicates that in addition to the thermodynamic analysis, economic and environmental impact assessment of a refrigeration system is indispensable nowadays, considering the rampant energy crisis and environmental degradation. However, to the best knowledge of the authors, only a few studies have been conducted on TCRS and those have mainly concentrated on 1st law efficiency and 2nd law efficiency. A thorough investigation into thermo-economic, environmental aspects and subsequent MOO of a TCR system has yet to be conducted, which inhibits the advancement of this sector. Hence, this study concentrates on assessing a TCRS (installed with hydrocarbon refrigerants) from the perspectives of thermodynamics, economics, and environmental impact, as well as determining the optimal operating condition via MOO. To comprehend the effect of various parameters on three objective functions (COP, exergy efficiency, and overall plant cost), a parametric analysis has been performed. To perform the optimization task, quadratic equations that map the input with the output objective function have been generated using the Box Behnken method in Minitab software, and based on these equations, multi-objective genetic algorithm (MOGA) in MATLAB® has been utilized to perform the optimization. TOPSIS and LINMAP decision techniques have been employed to extract a unique

Table 1
Relevant works employing MOO in the CRS system.

References	System	Refrigerants	Optimization method	Input Parameters	Optimized Parameters	Decision Technique
Patel et al. [56]	Double CRS	LTC: R1233zd(E) HTC: R41/R170	Heat transfer search	T_{evap}, T_{cond}, T_{LTC}, ΔT	Exergy efficiency, total plant cost	TOPSIS
Roy et al. [57]	Double CRS	LTC: R41, R170 HTC: R404A, R161	MOGA in MATLAB®	T_{evap}, T_{cond}, T_{LTC}, ΔT	Exergy efficiency, total plant cost	TOPSIS
Aminyavari et al. [58]	Double CRS	LTC: CO_2 HTC: NH_3	MOGA in MATLAB®	T_{evap}, T_{cond}, T_{LTC}, ΔT	Exergy efficiency, total plant cost	TOPSIS
Eini et al. [59]	Double CRS	LTC: CO_2 HTC: C_3H_8/NH_3	NSGA-II	T_{evap}, T_{cond}, T_{LTC}, ΔT	Exergy efficiency, total plant cost, total risk level	TOPSIS, LINMAP, Shannon's entropy
Singh et al. [60]	Double CRS with flash gas removal & flash intercooling	R717, R290, R1270, R744a, R600a	MOGA in MATLAB®	T_{evap}, T_{cond}, T_{LTC}, ΔT, subcooling parameter, a, superheating parameter, b	Exergy efficiency, total plant cost	TOPSIS
Nasruddin et al. [61]	Double CRS	HTC: C_3H_8 LTC: C_2H_6/CO2 mixture	MOGA in MATLAB®	T_{evap}, T_{cond}, T_{LTC}, ΔT, CO_2 mass fraction	Total annual cost, total exergy destruction	Avg. of the two best solutions

solution from the Pareto Front, and finally, the overall performance, flow of energy across the system, exergy destruction, and overall cost for each of the components have been evaluated at the optimum condition to assess the improvement potential of the plant. Through the comprehensive analysis of the TCRS via simulation, this study aims to make a significant contribution to the advancement of practical refrigeration systems designed for ultra-low temperature applications. Specifically, it focuses on applications such as the storage of vaccines and medicines in the pharmaceutical sector, food preservation in supermarkets, and diverse industrial processes, including the liquefaction of natural gas and petroleum gas.

2. Description of the TCRS

For ultra-low temperature (ULT) (−50 °C to −180 °C) applications, single/double stage VCR is infeasible due to poor volumetric efficiency of compressors, increased power demand, compressor failure, air leakage, and the need for robust pipe connectors, all these lead to poor COP and increased plant cost. TCRS, which is still in its nascent stages, can circumvent all these issues. Therefore, it is of the utmost importance to conduct a thorough analysis of this system from a variety of perspectives to determine its optimal operating condition. Fig. 1 depicts the schematic diagram of the TCR system which is comprised of three distinct VCR systems operating in distinct temperature ranges and connected by two cascade heat exchangers in between the VCR cycles. The VCR cycles are termed as Low temperature circuit (LTC), Mid temperature circuit (MTC) and High temperature circuit (HTC) based on their operating temperature level. The circuit that operates at the lowest temperature region is known as LTC, which is connected to the MTC via a cascade heat exchanger (CHX1) comprised of an LTC condenser and an MTC evaporator. Similarly, MTC is connected to HTC via another heat exchanger (CHX2), which operates at the highest temperature level in this system. The evaporator, throttle, compressor, and condenser are the four basic components in each of the deployed VCR systems in this study. So, the LTC evaporator and HTC condenser act as evaporators and condensers for the whole TCR system. Selected refrigerants for LTC, MTC, and HTC are 1-butene (C4H8), Heptane (C7H16), and m-Xylene (C8H10), respectively, and the specifications of these refrigerants are listed in Table 2.

The *T-s* and *P-h* diagram of the TCR cycle are illustrated in Fig. 2 (a) and (b) respectively. From the cold space, air enters into the evaporator at an inlet temperature, $T_{evapa,in}$ (state 13) and leaves at an outlet temperature, $T_{evapa,out}$ (state 14) after rejecting heat, $\dot{Q}_{evap}$ and LTC evaporator takes this heat at the evaporator temperature, T_{evap} to change its phase from state 4 to saturated vapor at state 1. Utilizing the required power, LTC compressor raises the pressure of this saturated vapor from state 1 to superheated vapor at state 2. This superheated refrigerant at state 2 enters the CHX I where it releases heat, $\dot{Q}_{CHX\ I}$ at constant pressure corresponding to LTC condenser temperature, T_{LTC} to change its phase to saturated liquid at state 3 and this heat is taken by MTC evaporator. The isenthalpic expansion through LTC throttling device drops the pressure from state 3 (condenser pressure) to state 4 (evaporator pressure) and thus completes the LTC. Similarly, MTC begins with evaporator in which MTC refrigerant's phase changes from state 8 to saturated vapor at state 5 by consuming the rejected heat from LTC. Temperature difference between LTC condenser and MTC evaporator or MTC condenser and LTC evaporator is cascade condenser temperature difference, ΔT. This saturated vapor is pressurized (state 5–6) to become superheated vapor at state 6 by MTC compressor utilizing input energy, $\dot{W}_{MTCC}$. This superheated steam changes its phase to become saturated liquid at state 7 in the CHX2 at a constant pressure corresponding to the temperature, T_{MTC} by releasing heat, $\dot{Q}_{CHX2}$ which is absorbed by HTC evaporator. The MTC completes with the MTC throttling device expanding the MTC refrigerant from state 7 to MTC evaporator pressure at state 8. HTC evaporator absorbs heat, $\dot{Q}_{CHX2}$ to change the phase of the HTC refrigerant from state 12 to become saturated vapor at state 9. HTC compressor raises its pressure to state 10 by absorbing compressor work input, $\dot{W}_{HTCC}$. In the condenser, the phase change of the HTC refrigerant from superheated vapor (state 10) to saturated liquid (state 11) occurs at a constant pressure corresponding to the condenser temperature, T_{cond} by releasing heat, $\dot{Q}_{cond}$ to the atmospheric air stream that enters the condenser at an inlet temperature, $T_{conda,in}$ and leaves it at $T_{conda,out}$. Finally, the isenthalpic expansion through the HTC throttle drops

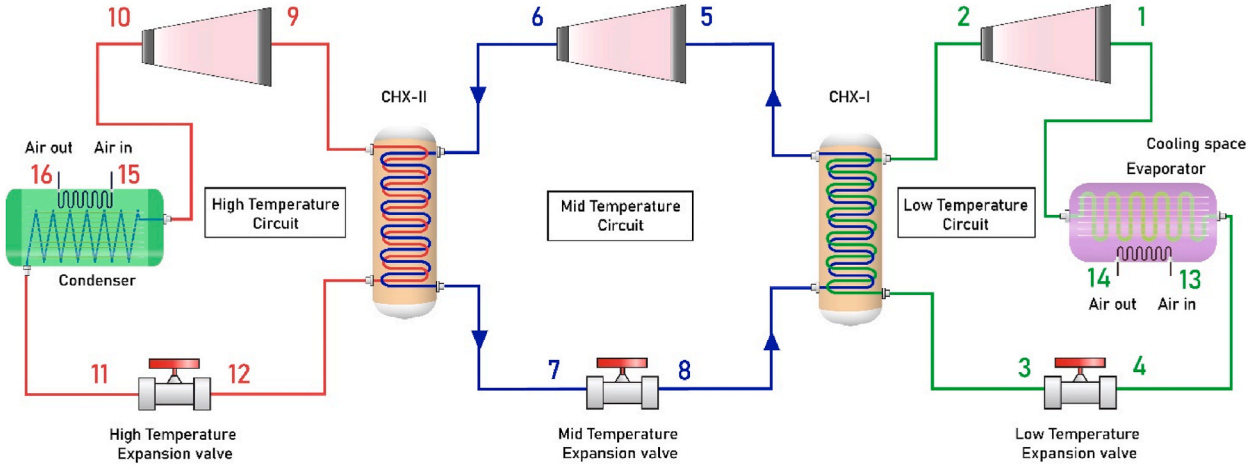

Fig. 1. Schematic diagram of the considered TCRS.

Table 2
Thermo-physical properties of selected refrigerants [41].

Characteristics of the refrigerants	1-butene	Heptane	m-Xylene
Molecular weight $\left(\text{kgkmol}^{-1}\right)$	56.11	100.2	106
Critical Temperature $(^{\circ}C)$	146.13	266.97	343.73
Critical Pressure (KPa)	4.01	2.73	3.53
Freezing Point $(^{\circ}C)$	−185.3	−90.6	−47.8
Vapor Density (Air = 1)	1.93	3.45	3.66
Heat of Vaporization $\left(\text{kjmol}^{-1}\text{ at }25\,^{\circ}C\right)$	20.31	36.57	42.65
GWP	20	20	20
ODP	0	0	0

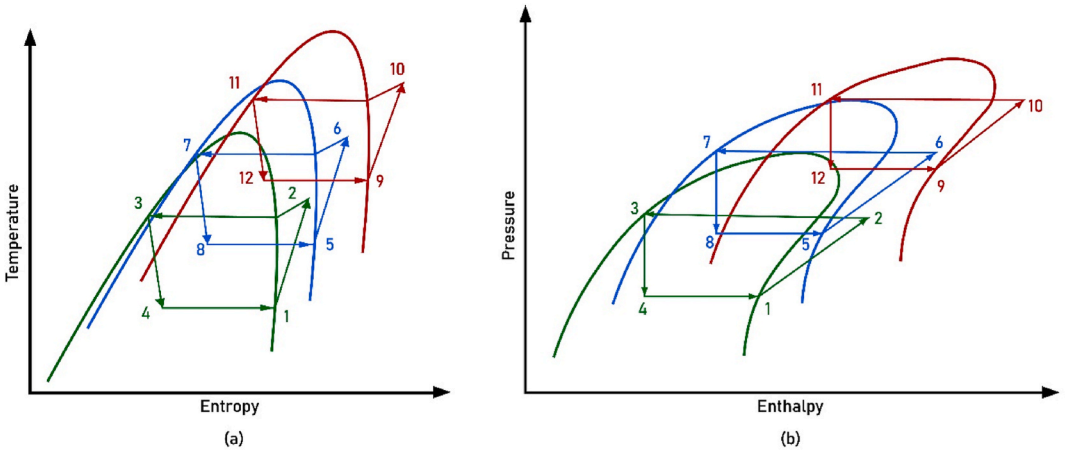

Fig. 2. (a) T-S diagram (b) P-h diagram of the TCRS.

the pressure from state 11 to state 12 (at HTC evaporator pressure) to complete the overall system.

3. Mathematical modelling

All the components of the TCRS under consideration have been modeled mathematically, and the corresponding equations have been developed in this section. The model has been analyzed from thermodynamic and economic perspectives. Based on some assumptions utilized in earlier works, the overall TCR modelling procedure can be simplified [62,63]. These assumptions are as follows:

- In this study, steady state & steady flow conditions are assumed for all the cycle's components.
- Neither the heat loss nor the pressure drops in the components and connecting pipes of the TCR system are taken into consideration.
- The electricity requirement for the evaporator and condenser fan is considered negligible.
- The thermodynamic processes of compressors and expansion valves are considered adiabatic.
- Heat exchangers used in this system are considered to have insignificant heat losses to the environment.
- The outlet condition for the condenser and both CHX are considered as saturated liquid while it is saturated vapor for the evaporator.
- For the condenser and evaporator, air is used as an external heat exchanging medium. The difference between the inlet and outlet temperature of the air is considered as 10k.

3.1. Energy & exergy analysis

For the kth component, mass and energy balance equations can be expressed as:

$$\sum_{k}(\dot{m})_{in} = \sum_{k}(\dot{m})_{out} \tag{1}$$

$$\dot{Q}_k + \sum_{k}(\dot{m}h)_{in} = \dot{W}_k + \sum_{k}(\dot{m}h)_{out} \tag{2}$$

Exergy, which denotes the maximum work potential of any system, can be analyzed for the effective utilization of energy. Only physical exergy is considered in this work which can be determined using following equation for any point in the system [64]:

$$e_{PH} = [h(T_s, P_s) - h_0(T_0, P_0)] - T_0[\, s\,(T_s, T_s) - s_0(T_0, P_0)] \tag{3}$$

T_s, P_s represent temperature and pressure respectively of any state point in the system. T_0, P_0 represent dead state temperature and Pressure considered in this work.

Under the assumptions mentioned earlier, the generalized equations have been applied taking each of the components of the TCRS as control volume to derive mass balance, energy & exergy balance equations for the system and are presented in Table 3. The equations related to the cycle performance assessment are listed in Table 4.

3.2. Economic analysis

Economic analysis begins with defining the various costs required within the system. Capital & maintenance cost (C&M), operations cost and penalty cost because of CO_2 emissions sum up as the combined cost for the whole system. Therefore, overall plant cost:

$$\dot{C}_{Total} = \sum_{k} \dot{C}_k + \dot{C}_{env} + + \dot{C}_{OP} \tag{4}$$

Where $\dot{C}_k$ is the cost rate for capital and maintenance, $\dot{C}_{env}$ defines the penalty cost for release of CO_2 and $\dot{C}_{OP}$ is the operation cost rate. The cost functions are listed in Table 5. Cost related to capital investment & maintenance (C&M) of the system's components [57]:

$$\dot{C}_k = C_k \times \varphi \times CRF \tag{5}$$

Where, the maintenance factor of the plant is denoted by φ & capital recovery factor, also known as CRF can be determined using the following equation [66]:

Table 3
Energy and exergy analysis related equations.

Components	Mass Balance	Energy Equations [41]	Exergy Equations [65]		
			Exergy of fuel ($\dot{E}_{F,k}$)	Exergy of product ($\dot{E}_{P,k}$)	Exergy destruction ($\dot{E}_{D,k}$)
LTC Compressor	$\dot{m}_{LTC} = \dot{m}_1 = \dot{m}_2$	$\dot{W}_{LTCC} = \dot{m}_{LTC} \times \frac{(h_{2S} - h_1)}{\eta_i\, \eta_m\, \eta_e}$	$\dot{E}_{F,LTCC} = \dot{W}_{LTCC}$	$\dot{E}_{P,LTCC} = \dot{m}_{LTC}(e_2 - e_{1)}$	$\dot{E}_{D,LTCC} = \dot{E}_{F,LTCC} - \dot{E}_{P,LTCC}$
MTC Compressor	$\dot{m}_{MTC} = \dot{m}_5 = \dot{m}_6$	$\dot{W}_{MTCC} = \dot{m}_{MTC} \times \frac{(h_{6S} - h_5)}{\eta_i\, \eta_m\, \eta_e}$	$\dot{E}_{F,MTCC} = \dot{W}_{MTCC}$	$\dot{E}_{P,MTCC} = \dot{m}_{MTC}(e_6 - e_{5)}$	$\dot{E}_{D,MTCC} = \dot{E}_{F,MTCC} - \dot{E}_{P,MTCC}$
HTC Compressor	$\dot{m}_{HTC} = \dot{m}_9 = \dot{m}_{10}$	$\dot{W}_{HTCC} = \dot{m}_{HTC} \times \frac{(h_{10S} - h_9)}{\eta_i\, \eta_m\, \eta_e}$	$\dot{E}_{F,HTCC} = \dot{W}_{HTCC}$	$\dot{E}_{P,HTCC} = \dot{m}_{HTC}(e_{10} - e_{9)}$	$\dot{E}_{D,HTCC} = \dot{E}_{F,HTCC} - \dot{E}_{P,HTCC}$
LTC Expansion Valve	$\dot{m}_{LTC} = \dot{m}_3 = \dot{m}_4$	$h_3 = h_4$	$\dot{E}_{F,LTC,TV} = \dot{m}_{LTC} e_3$	$\dot{E}_{P,LTC,TV} = \dot{m}_{LTC} e_4$	$\dot{E}_{D,LTC,TV} = \dot{E}_{F,LTC,TV} - \dot{E}_{P,LTC,TV}$
MTC Expansion Valve	$\dot{m}_{MTC} = \dot{m}_7 = \dot{m}_8$	$h_7 = h_8$	$\dot{E}_{F,MTC,TV} = \dot{m}_{MTC} e_7$	$\dot{E}_{P,MTC,TV} = \dot{m}_{MTC} e_8$	$\dot{E}_{D,MTC,TV} = \dot{E}_{F,MTC,TV} - \dot{E}_{P,MTC,TV}$
HTC Expansion Valve	$\dot{m}_{HTC} = \dot{m}_{11} = \dot{m}_{12}$	$h_{11} = h_{12}$	$\dot{E}_{F,HTC,TV} = \dot{m}_{HTC} e_{11}$	$\dot{E}_{P,HTC,TV} = \dot{m}_{HTC} e_{12}$	$\dot{E}_{D,HTC,TV} = \dot{E}_{F,HTC,TV} - \dot{E}_{P,HTC,TV}$
Cascade Heat Exchanger I	$\dot{m}_{LTC} = \dot{m}_2 = \dot{m}_3$ $\dot{m}_{MTC} = \dot{m}_5 = \dot{m}_8$	$\dot{Q}_{CHX\ I} = \dot{m}_{MTC} \times (h_5 - h_8)$ $\dot{Q}_{CHX\ I} = \dot{m}_{ltc} \times (h_2 - h_3)$	$\dot{E}_{F,CHX\ I} = \dot{m}_{LTC}(e_2 - e_5)$	$\dot{E}_{P,CHX\ I} = \dot{m}_{MTC}(e_3 - e_8)$	$\dot{E}_{D,CHX\ I} = \dot{E}_{F,CHX\ I} - \dot{E}_{P,CHX\ I}$
Cascade Heat Exchanger *II*	$\dot{m}_{MTC} = \dot{m}_6 = \dot{m}_7$ $\dot{m}_{htc} = \dot{m}_9 = \dot{m}_{12}$	$\dot{Q}_{CHX\ II} = \dot{m}_{MTC} \times (h_6 - h_7)$ $\dot{Q}_{CHX\ II} = \dot{m}_{htc} \times (h_9 - h_{12})$	$\dot{E}_{F,CHX\ II} = \dot{m}_{MTC}(e_6 - e_9)$	$\dot{E}_{P,CHX\ II} = \dot{m}_{HTC}(e_7 - e_{12})$	$\dot{E}_{D,CHX\ II} = \dot{E}_{F,CHX\ II} - \dot{E}_{P,CHX\ II}$
Evaporator	$\dot{m}_{LTC} = \dot{m}_1 = \dot{m}_4$ $\dot{m}_{air,evp} = \dot{m}_{13} = \dot{m}_{14}$	$\dot{Q}_{evap} = \dot{m}_{LTC} \times (h_1 - h_4)$	$\dot{E}_{F,evap} = \dot{m}_{LTC}(e_4 - e_1)$	$\dot{E}_{P,evap} = \dot{m}_{eva}(e_{14} - e_{13})$	$\dot{E}_{D,evap} = \dot{E}_{F,evap} - \dot{E}_{P,evap}$
Condenser	$\dot{m}_{HTC} = \dot{m}_{10} = \dot{m}_{11}$ $\dot{m}_{air,cond} = \dot{m}_{15} = \dot{m}_{16}$	$\dot{Q}_{cond} = \dot{m}_{HTC} \times (h_{10} - h_{11})$	$\dot{E}_{F,cond} = \dot{m}_{HTC}(e_{10} - e_{11})$	$\dot{E}_{P,cond} = \dot{m}_{conda}(e_{16} - e_{15})$	$\dot{E}_{D,cond} = \dot{E}_{F,cond} - \dot{E}_{P,cond}$

Table 4
Cycle Performance related equations.

Parameters	Equation [41]
Overall system COP	$COP = \frac{\dot{Q}_{evap}}{\dot{W}_{total}}$
Total Work input	$\dot{W}_{total} = \dot{W}_{LTCC} + \dot{W}_{MTCC} + \dot{W}_{HTCC}$
Total Exergy Destruction	$\dot{E}_{D,total} = \dot{E}_{D,LTCC} + \dot{E}_{D,MTCC} + \dot{E}_{D,HTCC} + \dot{E}_{D,LTC,TV} + \dot{E}_{D,MTC,TV} + \dot{E}_{D,HTC,TV} + \dot{E}_{D,CHX\ I} + \dot{E}_{D,CHX\ II} + \dot{E}_{D,evap} + \dot{E}_{D,cond}$
LTC COP	$COP_{LTC} = \frac{\dot{Q}_{CHX\ I}}{\dot{W}_{LTCC}}$
MTC COP	$COP_{MTC} = \frac{\dot{Q}_{CHX\ II}}{\dot{W}_{MTCC}}$
HTC COP	$COP_{HTC} = \frac{\dot{Q}_{evap}}{\dot{W}_{HTCC}}$
Exergy Efficiency	$\eta = 1 - \frac{\dot{E}_{D,total}}{\dot{W}_{total}}$

Table 5
Cost function for each component in the cycle.

Components		Cost function [58,67]
HTC	Compressor	$C_{HTCC} = 9624.2 \times W_{HTCC}^{0.46}$
	Throttle valve	$C_{TV,HTC} = 114.5 \times \dot{m}_{HTC}$
LTC	Compressor	$C_{LTCC} = 10167.5 \times W_{LTCC}^{0.46}$
	Throttle valve	$C_{TV,LTC} = 114.5 \times \dot{m}_{LTC}$
MTC	Compressor	$C_{MTCC} = 9895.85 \times W_{MTCC}^{0.46}$ [avg. of LTC & HTC]
	Throttle Valve	$C_{TV,MTC} = 114.5 \times \dot{m}_{MTC}$
Evaporator		$C_{evap} = 1397 \times A_{evap}^{0.89}$
Condenser		$C_{cond} = 1397 \times A_{cond}^{0.89}$
Cascade condenser I		$C_{CHX\ 1} = 383.5 \times A_{CHX\ 1}^{0.65}$
Cascade condenser *II*		$C_{CHX\ 2} = 383.5 \times A_{CHX\ 2}^{0.65}$

$$CRF = \frac{in_r(in_r+1)^n}{(in_r+1)^n - 1} \tag{6}$$

Where, in_r is the rate of interest, n is plant's lifetime. Evaporator, both CHX and condenser heat transfer area can be determined as follows [67]:

$$A = \frac{\dot{Q}}{U \times LMTD} \tag{7}$$

Here,

U = Overall heat transfer coefficient.

$\dot{Q}$ = Total heat transfer rate

LMTD can be expressed as:

$$LMTD = \frac{(T_{h1} - T_{c2}) - (T_{h2} - T_{c1})}{\ln\frac{(T_{h1} - T_{c2})}{(T_{h2} - T_{c1})}} \tag{8}$$

Hot stream inlet and outlet temperature are denoted by T_{h1}, T_{h2} respectively and cold stream inlet and outlet temperature are denoted by T_{c1}, T_{c2} respectively. The cost rate of operation mainly includes the cost required to run the compressor which is expressed as:

$$\dot{C}_{op} = N \times W_{Total} \times \propto_{electricity} \tag{9}$$

Here, W_{Total} = total compressor work and $\propto_{electricity}$ = Electrical Power Cost

Total capital & maintenance (C&M) cost can be estimated by summing up all the components' C&M costs.

$$\sum_k \dot{C}_k = \dot{C}_{evap} + \dot{C}_{cond} + \dot{C}_{CHX\ 1} + \dot{C}_{CHX\ 2} + \dot{C}_{HTCC} + \dot{C}_{LTCC} + \dot{C}_{MTCC} + \dot{C}_{TV,LTC} + \dot{C}_{TV,MTC} + \dot{C}_{TV,HTC} \tag{10}$$

3.3. Environmental impact analysis

The system's penalty cost rate associated with GHG emission can be determined by applying the following equation [68]:

$$\dot{C}_{env} = m_{CO_2e} \times C_{CO_2} \tag{11}$$

Here,

C_{CO_2} = Cost associated with avoiding CO_2

m_{CO_2e} = mass of yearly discharged GHG

$$m_{CO_2e} = \mu_{CO_2e} \times E_{Annual} \tag{12}$$

Here,

μ_{CO_2e} = Emission Factor

E_{Annual} = yearly power requirement

3.4. Selection of input parameters with their corresponding ranges

The selection of input and output parameters has been grounded in a comprehensive literature review and the justification for this choice is further substantiated through the application of a correlation matrix (shows the correlation of the input and output parameters) in the later sections. The determination of input parameters' ranges is based on pertinent studies on TCRS, specifically the works of Faruque et al. [41], Nabil et al. [69], Sun et al. [10] and Wang et al. [70]. In addition to the previous works on TCRS, the selection is significantly influenced by the practical applicability of the proposed system. Despite the purely simulation-based nature of this work, the overarching objective is to contribute to the advancement of practical refrigerators dedicated to ultra-low temperature (ULT) applications. As such, the evaporator temperature has been varied to enhance its suitability for a broad range of ULT applications. The selection of the condenser temperature range has been determined with a focus on practical applicability as well. The design parameters utilized in this simulation have been listed in Table 6.

Finally, employing the Python programming language, a mathematical model capable of simulating the variations of several performance-evaluating parameters such as COP, exergy efficiency, total equivalent CO_2 emission, total plant cost rate, with respect to T_{evap}, T_{cond}, T_{LTC}, T_{MTC}, ΔT of the proposed system has been developed. CoolProp, a dedicated Python Library is employed to determine the refrigerants' thermodynamic properties at different states. Fig. 3 depicts the overall modelling procedure employed in this work.

4. Validation of the proposed model

4.1. Validation of energy analysis

The presented model has been compared to the work of Faruque et al. [41] under similar operating conditions as listed in Table 7. The comparison between the presented model and reference model is presented in Fig. 4 and Table 8 lists the deviations, MAPE, RSME and R^2 scores. With deviations consistently well below the accepted threshold and error metrics falling within a reasonable range, it is

Table 6
Design parameters for the optimization of the presented model.

System Parameters			Selected Values
Dead State	Temperature, T_0		25 °C
	Pressure, P_0		101.3 kPa
Cooling Load			**10 kW**
Compressor	Isentropic Efficiency, η_i		80 %
	Electrical Efficiency, η_e		100 %
	Mechanical Efficiency, η_m		100 %
Range for the simulation	Evaporator Temperature, T_{evap}		−140 °C to −101 °C
	Condenser Temperature, T_{cond}		36 °C to 60 °C
	Cascade Condenser I Temperature difference, ΔT		4 °C to 8 °C
	LTC Condenser Temperature, T_{LTC}		−80 °C to −40 °C
	MTC Condenser Temperature, T_{MTC}		−35 °C to 10 °C
Inlet Air Temperature	to the Evaporator		−90 °C
	to the Condenser		25 °C
Outlet Air Temperature	from the Evaporator		−100 °C
	from the Condenser		35 °C
Plant's lifetime, n			15 years [57,67]
Maintenance factor of the plant, φ			1.06 [57,67]
Interest rate, in_r			14 % [57,67]
Hours of operation per year, N			4266 h [57,67]
Overall heat transfer coefficient, U		Evaporator	30 $Wm^{-2}K^{-1}$ [57,67]
		Condenser	40 $Wm^{-2}K^{-1}$ [57,67]
		Cascade Condenser	1000 $Wm^{-2}K^{-1}$ [57,67]
Emission Factor, $\mu_{CO_2}e$			0.968 kg/kW h [57,67]
Cost associated with avoiding CO_2, C_{CO_2}			0.090 $/kg release of CO_2 [57]
Cost of electricity, α_{el}			0.090 $/kWh [57,67]

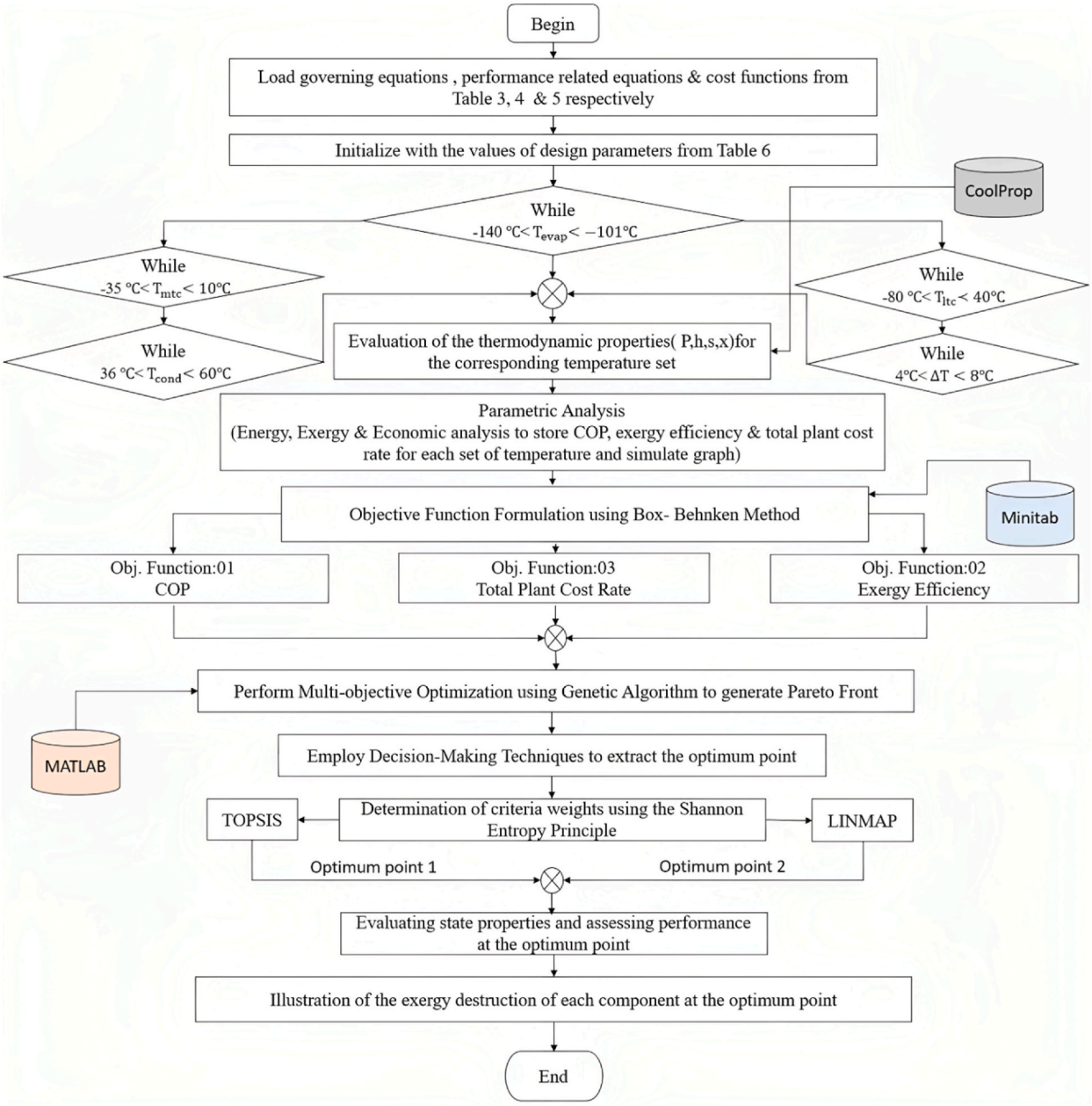

Fig. 3. Flowchart of overall modelling procedure.

substantiated that the presented model aptly reproduces the functions of the reference model.

4.2. *Economic analysis validation*

A mathematical model has been constructed to validate the economic analysis, and the results have been contrasted to those of Roy et al. [57] in the identical condition. Validation has been done for the double cascade VCR system as there wasn't any earlier work related to the economic analysis of a TCR system. Fig. 5 depicts the comparison between the presented model and reference model in terms of variation in the rate of total plant with LTC evaporator temperature. The presented model is well fitted with the reference model as maximum percentage of deviation is around 2.24 %. Furthermore, the calculated MAPE, RMSE, and R^2 score values collectively indicate a high level of accuracy and reliability of the presented model, as listed in Table 9. The minimal errors observed in this study may be attributed to the utilization of an alternative library, CoolProp, for the determination of enthalpy and entropy at each state.

Table 7
Considered Parameters for the validation of the simulated model [41].

Parameters		Values
Ambient	Temperature, T_{amb}	25 °C
	Pressure, P_{amb}	101.325 kPa
Cooling Load, Q_{evap}		10 kW
Condenser Temperature, T_{cond}		40 °C
Evaporator Temperature, T_{evap}		−100 °C
LTC Condenser Temperature, T_{LTC}		−80 °C to −40 °C
MTC Condenser Temperature, T_{MTC}		−15.6 °C
Cascade Temperature difference, Δ T		5 °C
Compressor	Isentropic Efficiency, η_i	0.80
	Mechanical Efficiency, η_m	0.90
	Electrical Efficiency, η_e	0.95

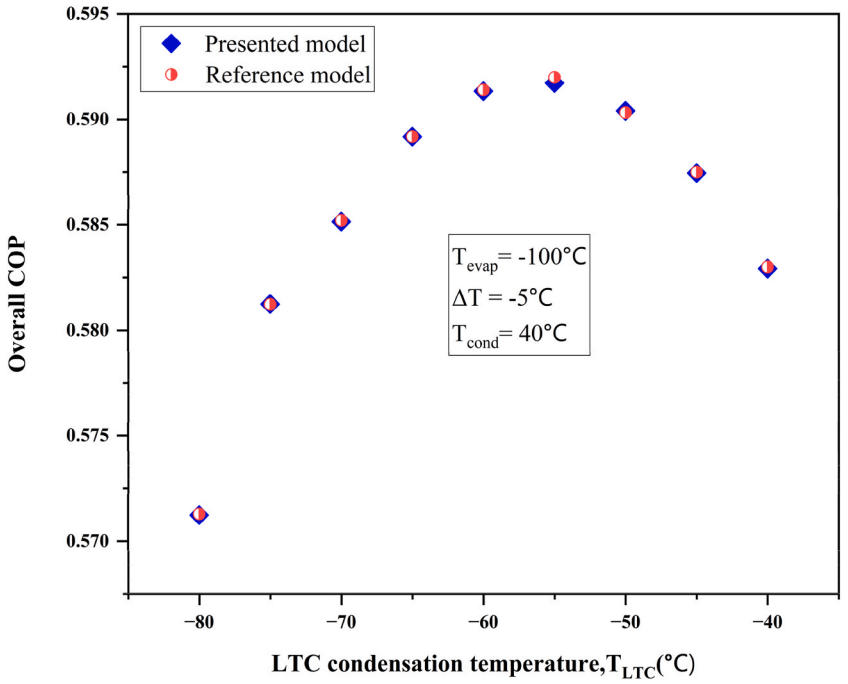

Fig. 4. Comparison of the presented simulation model with Faruque et al. [41].

Table 8
Validation of the thermodynamic model.

T_{LTC} (°C)	Presented model COP	Reference model COP [41]	Deviation (%)	MAPE	RSME	R^2
−80	0.5712	0.5713	0.011	**0.00013**	**0.000108**	**0.999**
−75	0.5813	0.5812	0.002			
−70	0.5852	0.5852	0.009			
−65	0.5892	0.5892	0.002			
−60	0.5913	0.5914	0.010			
−55	0.5917	0.5920	0.047			
−50	0.5904	0.5903	0.015			
−45	0.5875	0.5875	0.009			
−40	0.5829	0.5830	0.014			

4.3. Experimental validation

The model has been validated with the previous simulation models, both using energy analysis and economic analysis. However, it is necessary to validate the simulated model with previously conducted experimental studies to enhance the robustness and reliability

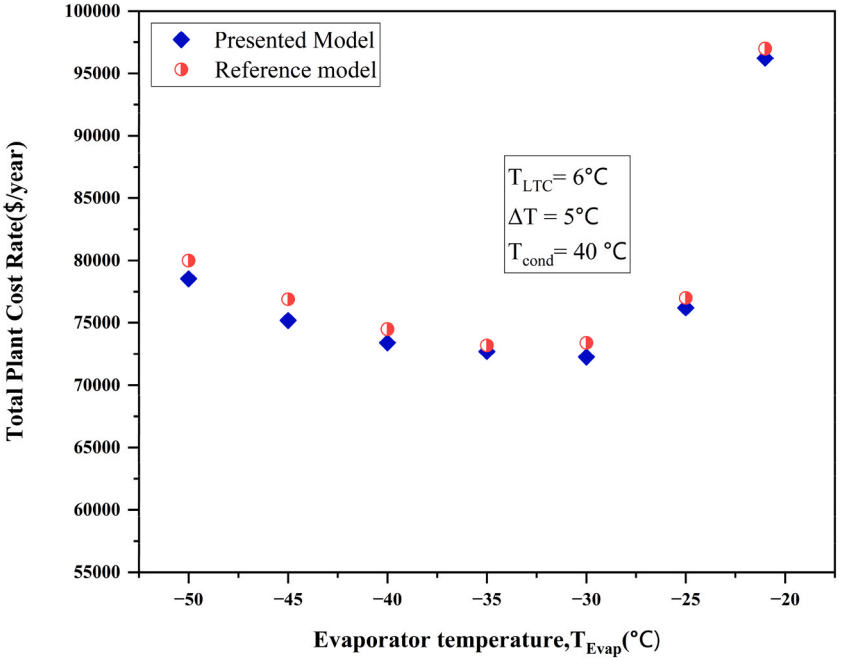

Fig. 5. Economic analysis validation of the presented model with Roy et al. [57].

of the model. As experimental works on the TCR system are yet to be conducted, experimental validation has been performed using a single-stage VCR system. The operational parameters considered for validation have been listed in Table 10. The COP for both the experimental and presented models has been compared in Table 11, employing error metrics and relative deviations. The MAPE, RMSE, and relative deviations all fall well within acceptable ranges, while the R^2 value indicates a robust fit between the presented and experimental models. Fig. 6 illustrates the COP variation with evaporator temperature for both the experimental setup and the presented model, demonstrating the close alignment and adherence of the presented model to the experimental trend.

5. Optimization of the system

5.1. Multi objective optimization (MOO)

MOO is a widely used method for resolving practical problems involving multiple conflicting objectives, such as maximizing efficiency while minimizing the cost. There is no unique solution for these types of problems which can simultaneously satisfy each of the objectives, rather non-dominated solutions' set which make the Pareto optimal set are generated by making the best tradeoff between the conflicting objectives by employing this approach [72,73]. Afterward, several decision-making techniques are employed by the decision makers to identify a unique solution from the Pareto front.

5.1.1. Objective function formulation using Box-Behnken method

Box-Behnken design (BBD) is a broadly utilized statistical experimental design technique in response surface methodology (RSM) for correlating multiple input variables with a response variable [74]. It operates by fitting a response surface using regression techniques while requiring fewer experimental trials than a full factorial design, making it a valuable tool for researchers to generate quadratic equations that efficiently relate a response variable to multiple operating variables and afterward conduct optimization tasks [75]. In this work, the quadratic equations for the considered objective functions (rate of total plant cost, COP & exergy efficiency)

Table 9
Validation of the economic model.

T_{Evap} (°C)	Presented model Cost ($/year)	Reference model Cost ($/year) [57]	Deviation (%)	MAPE	RSME	R^2
−50	78530	80000	1.84	**0.014**	**1142.7**	**0.98**
−45	75178	76900	2.24			
−40	73400	74500	1.48			
−35	72700	73200	0.68			
−30	72250	73400	1.57			
−25	76200	77000	1.04			
−21	96230	97000	0.79			

Table 10
Considered operational parameters for the experimental validation [71].

Parameters	Values
Refrigerant	R134a
T_{evap}	$-15\ ^{\circ}C$ to $-5\ ^{\circ}C$
T_{cond}	$40\ ^{\circ}C$
Degree of sub-cooling in the condenser	$2.4\ ^{\circ}C$
Degree of superheating in the evaporator	$10.6\ ^{\circ}C$
Compressor efficiency (%)	63 % at $T_{evap} = -15\ ^{\circ}C$ 54 % at $T_{evap} = -10\ ^{\circ}C$ 45 % at $T_{evap} = -5\ ^{\circ}C$

Table 11
Comparison of the presented model and the experimental work of Ma et al. [71].

T_{evap} ($^{\circ}C$)	COP		Deviation (%)	MAPE	RSME	R^2
	Experimental Model [71]	Presented Model				
−15	1.61	1.63	1.24	0.00934	0.02	0.998799
−10	2.23	2.25	0.896			
−5	3.02	3.04	0.662			

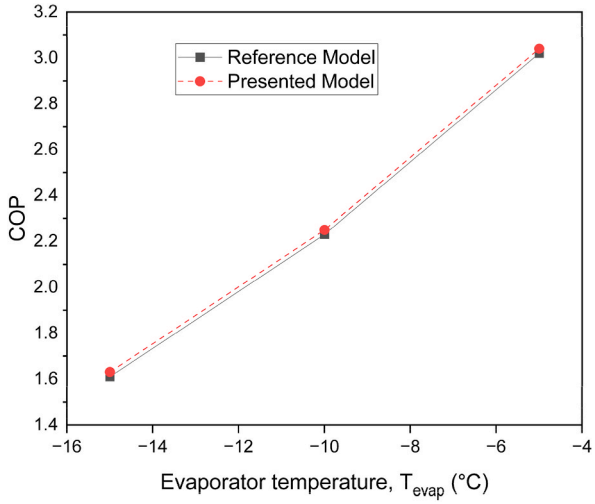

Fig. 6. Validation of the presented model with the experimental work of Ma et al. [71].

have been developed by correlating these to their operating parameters (T_{evap}, T_{LTC}, T_{MTC}, ΔT) using Box-Behnken design methodology in Minitab software. The design summary of the considered BBD is described in Table 12.

5.1.2. Optimization using genetic algorithm (GA)

GA operates on a mechanism that is identical to Darwin's laws of natural selection and nowadays it has become a popular technique to optimize multiple objectives simultaneously [76]. In this work, the *gamultiobj* solver of the optimization toolbox in MATLAB®

Table 12
BBD design parameters in Minitab.

Design Parameters	Value
Factors	4
Base runs	74
Base blocks	3
Replicates	50
Total runs	3700
Total blocks	150
Center points	2500

software is used for the optimization task of the equations that were generated in Minitab software for the considered objectives. Here, COP and exergy efficiency must be maximized while minimizing overall plant cost must. Selected values for different parameters in MATLAB® optimization toolbox are listed in Table 13. The optimization design parameters along with their ranges are listed in Table 14. The overall optimization procedure is illustrated in. Fig. 7.

5.2. Decision making technique

Although the Pareto Front represents the optimal solution set for the desired MOO task, the application of decision-making techniques can generate a unique solution based on the users' priority of objectives. This study compares the optimal value for two extensively employed decision making techniques: TOPSIS*(Technique for order preference by similarity to ideal solution)* [77] and LINMAP *(linear programming technique for multidimensional analysis of preference)* [78]; Shannon Entropy Principle [79] has been utilized for weight evaluation which are listed in Table 15 and these weights will be used in TOPSIS and LINMAP to rank all the alternatives.

6. Results and discussion

This study investigates a 10 kW TCRS from thermodynamic, economic, and environmental point of view. Initially, a parametric analysis has been performed to illustrate the influence of various parameters on system performance. The Box-Behnken method have been used then to construct quadratic equations that relate influential system parameters to the objective functions considered (COP, exergy efficiency, and total plant cost). Employing MOO, a Pareto Front has been generated for these objective functions, subsequently the TOPSIS and LINMAP decision making techniques have been used to derive a unique solution from the Pareto front. Finally, the performance of the entire system has been evaluated at the optimal point, and the exergy destruction of each component has been illustrated to reveal the potential for improvement.

6.1. Effect of evaporator temperature

Fig. 8 depicts the changes of the TCRS' *COP*, total work input (W_{total}), exergy efficiency (η) & exergy destruction ($E_{D,total}$) with evaporator temperature, T_{evap} ranging from $-140\ ^{\circ}C$ to $-104\ ^{\circ}C$ while holding other parameters constant at $T_{LTC} = -70\ ^{\circ}C$, $T_{MTC} = -30\ ^{\circ}C$, $T_{cond} = 40\ ^{\circ}C$ and $\Delta\ T = 5\ ^{\circ}C$. It has been observed that as evaporator temperature rises, both work input and exergy destruction decrease which causes exergy efficiency and overall COP to increase linearly. The rationale for this pattern is that, as T_{evap} rises, temperature elevation across the LTC compressor (LTCC) decreases which drops the required pressure ratio and ultimately both the required power and exergy destruction across the LTCC decrease and cause the COP & exergy efficiency to be increased. For a 35 °C decrease in evaporator temperature, compressor work and exergy destruction are observed to decrease by 47.5 % and 62.2 %, respectively, leading to a 91.2 % and 83.7 % increase in COP and exergy efficiency, respectively. This justifies the substantial effect of T_{evap} on system performance, with this parameter influencing COP ($0.009\ ^{\circ}C^{-1}$) slightly more than exergy efficiency ($0.006\ ^{\circ}C^{-1}$).

6.2. Effect of condenser temperature

The variations of the TCRS' *COP*, compresor work, W_{total}, exergy efficiency η and exergy destruction, $E_{D,total}$ with condenser temperature, T_{cond} ranging from $36\ ^{\circ}C$ to $58\ ^{\circ}C$ are illustrated in Fig. 9. It has been noticed that both the total compressor work and the exergy destruction rise as condenser temperature increases, consequently leading to a drop in COP and exergy efficiency. The primary reason for this deterioration in system performance is that as T_{cond} rises, more temperature elevation is required in HTC compressor (HTCC) which increases the HTCC pressure ratio, and all these increase the TCRS' input power and overall exergy destruction which deteriorate the performance (COP & exergy efficiency). Total compressor work increases by 20.3 % which results in a 15.7 % decline in overall COP for $22\ ^{\circ}C$ rises in T_{cond}, whereas 32 % increase in total exergy destruction is observed for similar operating condition which

Table 13
Selected Values for different parameters of Multi objective optimization algorithm.

Specified Options		Selected Value
Population Size		200
Creation Function		Constraint Dependent
Tournament Size		2
Crossover	function	Intermediate
	ratio	1
Migration	fraction	0.20
	direction	forward
Mutation	probability	Constraint dependent
	function	0.10
Distance Measure Function		Distancecrowding
Population fraction of the Pareto Front		0.35
Max. Tolerance	constraint	10^{-3}
	function	10^{-4}

Table 14
Optimization design parameters with their ranges.

Design Parameters	Range
Evaporator Temperature, T_{evap} ($^{\circ}C$)	$-140 \leq T_{evap} \leq -101$
LTC condenser Temperature, T_{LTC} ($^{\circ}C$)	$-80 \leq T_{ltc} \leq -40$
MTC condenser Temperature, T_{MTC} ($^{\circ}C$)	$-35 \leq T_{mtc} \leq 10$
Cascade Condenser Temperature difference, ΔT ($^{\circ}C$)	$4 \leq \Delta T \leq 8$
Condenser Temperature, T_{cond} ($^{\circ}C$)	$36 \leq T_{cond} \leq 60$

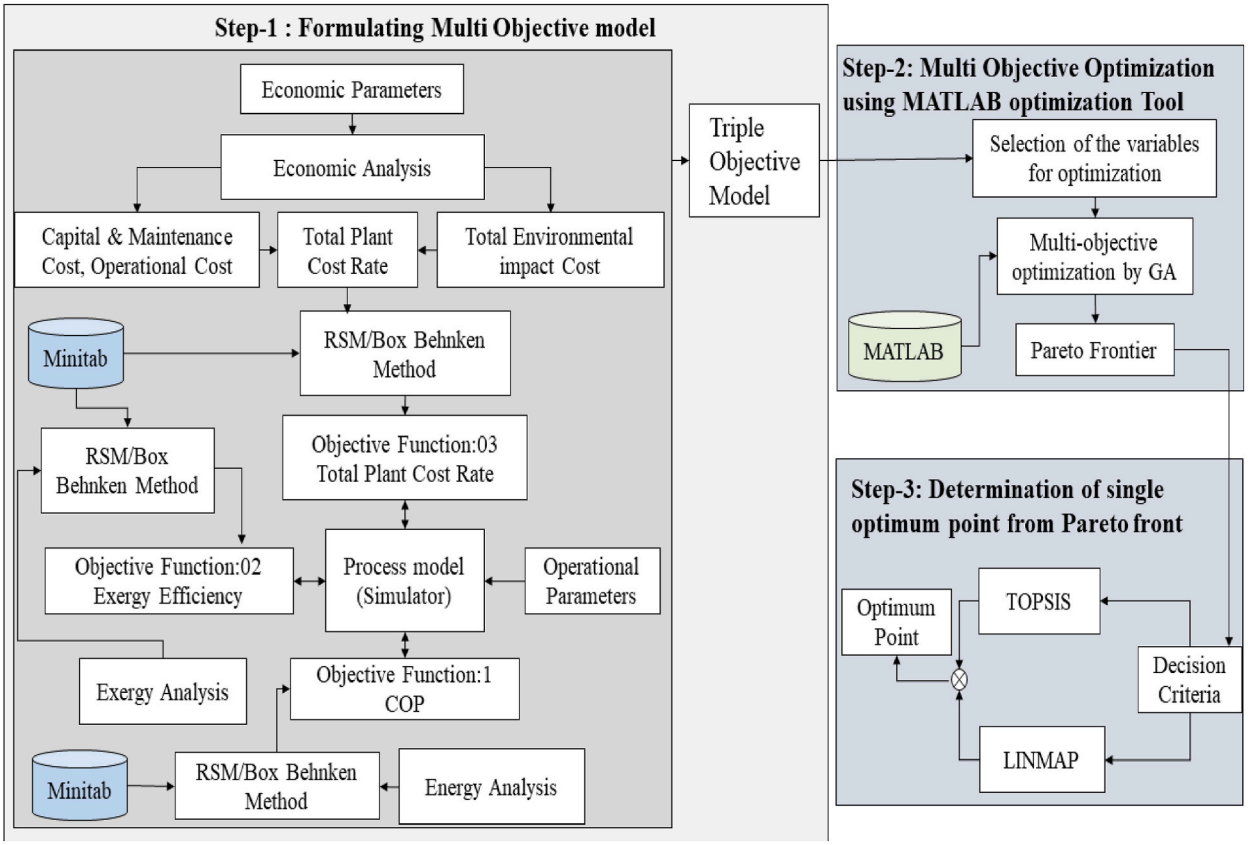

Fig. 7. Flow chart for triple objective optimization procedure.

Table 15
Generated weight of the criteria using the Shannon Entropy Principle.

Criteria	Weight
Total Plant Cost	0.15
Overall COP	0.45
Exergy Efficiency	0.40

leads to 16.2 % fall in exergy efficiency. It can be concluded that variation in T_{cond} equally affects COP (0.004 $^{\circ}C^{-1}$) and exergy efficiency (0.003 $^{\circ}C^{-1}$), although the impact is quite low compared to T_{evap}.

6.3. Effect of LTC condenser temperature

The changes of the TCRS' *COP*, compressor work, W_{total}, exergy efficiency, η and exergy destruction, $E_{D,total}$ with LTC condenser temperature, T_{LTC} ranging from $-80\ ^{\circ}C$ to $-44\ ^{\circ}C$ are depicted in Fig. 10. It demonstrates that both work input and exergy destruction decrease initially up to a specific temperature ($-76\ ^{\circ}C$), and after that, both parameters exhibit a quadratic increment with T_{LTC},

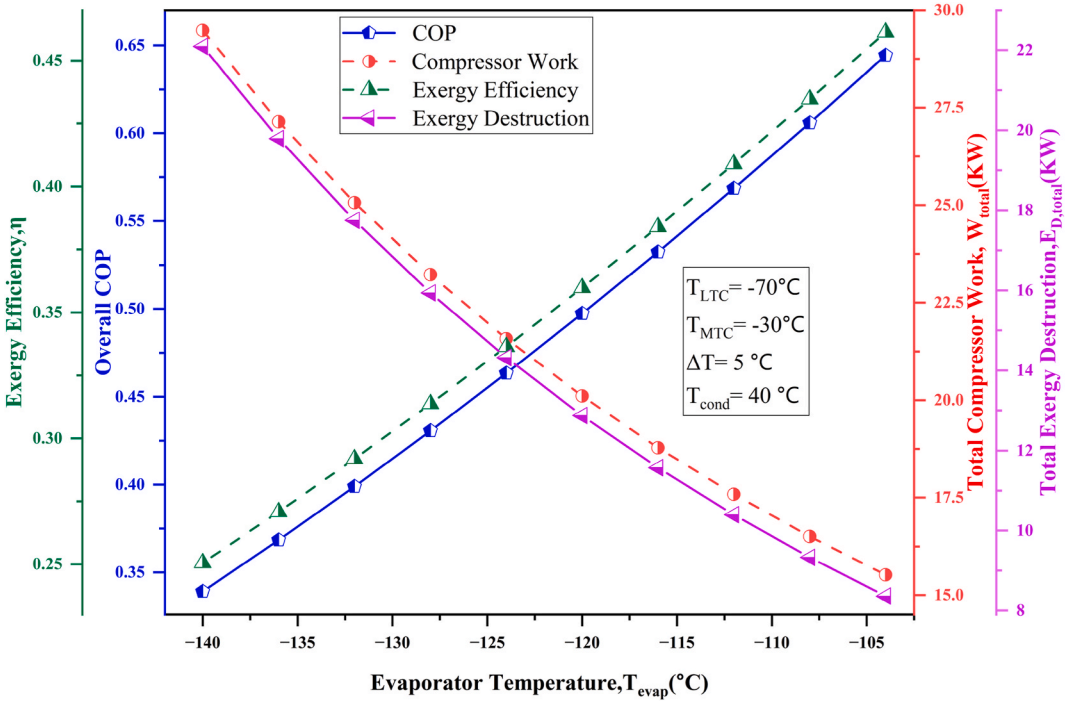

Fig. 8. Variations of energy (COP, W_{total}) & exergy (η, $E_{D,total}$) related parameters with T_{evap}.

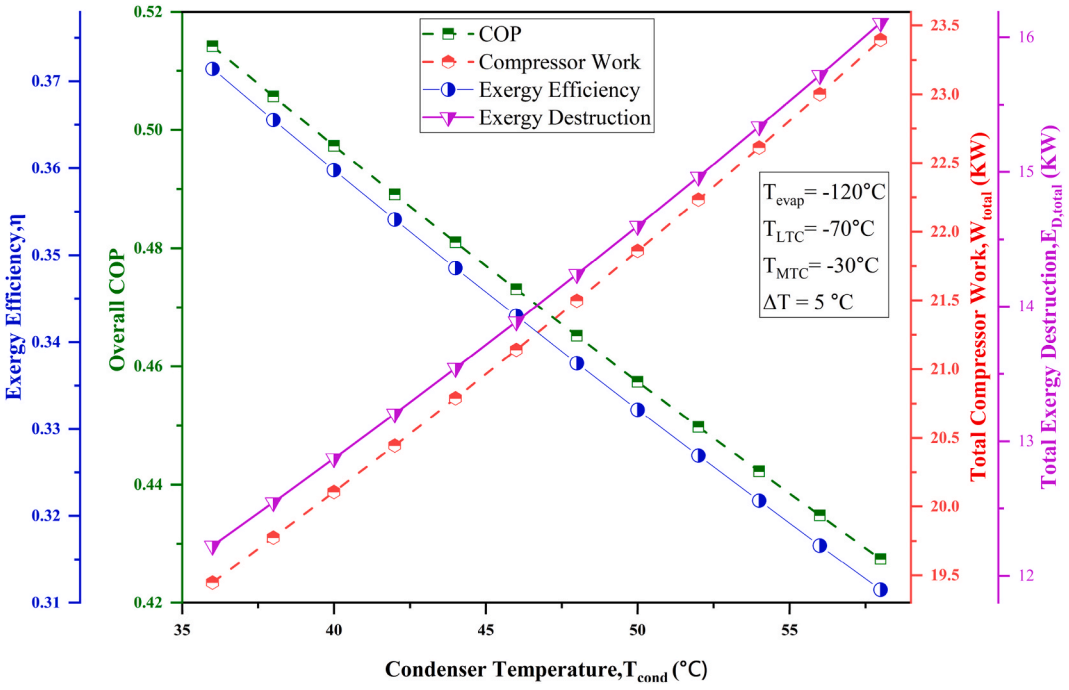

Fig. 9. Variations of Energy (COP, W_{total}) & Exergy (η, $E_{D,total}$) related parameters with T_{cond}.

whereas exactly opposite trend is observed for COP and exergy efficiency. The reason for this trend is that when T_{LTC} increases, LTCC pressure ratio rises, and MTC compressor (MTCC) pressure ratio drops. This causes the work input to rise in LTCC and fall in MTCC. The overall power requirement drops initially as the drop in the amount of work input in MTCC is greater than the rise of the same in LTCC. However, the increase rate in LTCC is higher than the decrease rate in MTCC. After a certain temperature, the increase of the work

input in LTCC surpasses the decrease of the same in MTCC, thus overall power requirement keeps increasing. For initial changes in T_{LTC} ($-80\ ^{\circ}C$ to $-76\ ^{\circ}C$), compressor work and exergy destruction drop at an avg. rate of 0.0033 kW/ $^{\circ}C$ and 0.0025 kW/ $^{\circ}C$ respectively while both COP and exergy efficiency increases at an avg. rate of 0.0025 $^{\circ}C^{-1}$. At the optimum temperature ($-76\ ^{\circ}C$), COP and exergy efficiency are 0.499 and 0.361 respectively. After that, compressor work and exergy destruction rise at an avg. rate of 0.03 kW/ $^{\circ}C$ and 0.034 kW/ $^{\circ}C$ respectively which leads to COP and exergy efficiency declining at an avg. rate of 0.0008 $^{\circ}C^{-1}$ and 0.0006 $^{\circ}C^{-1}$ respectively. It is evident that T_{LTC} has minimal impact on system performance at lower temperatures (up to $-76\ ^{\circ}C$), but then has a significant effect on COP and exergy efficiency, with a disproportionately large effect on COP.

6.4. Effect of MTC condenser temperature

Fig. 11 demonstrates the changes of the TCRS' COP, compressor work, W_{total}, exergy efficiency, η and exergy destruction, $E_{D,total}$ with MTC condenser temperature, T_{MTC} ranging from-35 °C to 9 °C. The values of T_{evap}, T_{cond}, T_{LTC}, Δ T have been kept at −120 °C, 40 °C, −60 °C, and 5 °C respectively throughout the simulation process. It is observed that initially both compressor work and exergy destruction show quadratic decrement with T_{MTC}, reaching their minimum value for a specific temperature, and after that, both exhibit quadratic increments. In contrast, COP and exergy efficiency exhibit the exact opposite trend. The driving factor behind this trend is that with the increase in T_{MTC}, the pressure ratio goes up in MTC compressor (MTCC) while it drops in HTCC, so does the power requirement. The overall power requirement drops initially as the required power's decrease in HTCC is larger than the rise in MTCC at this stage. But the increment rate in MTCC is higher than the decrement rate in HTCC. After a certain temperature (−15 °C), the increase in MTCC power requirement surpasses the decrease in HTCC power requirement, thus overall power requirement keeps increasing. Initially, compressor work and exergy destruction drop at an avg. rate of 0.031 kW/ $^{\circ}C$ and 0.03 kW/ $^{\circ}C$ respectively while COP and exergy efficiency rise at an avg. rate of 0.00073 $^{\circ}C^{-1}$ and 0.0005 $^{\circ}C^{-1}$ up to −15 °C. At the optimum point (−15 °C), compressor work (20.178 KW) and exergy destruction (12.942 kW) are at their minimum while COP (0.4956) and exergy efficiency (0.359) are at their maximum. After that, both compressor work and exergy destruction continue to increase at an avg. rate of 0.02 kW/ $^{\circ}C$ while COP and exergy efficiency maintain an avg. Decrement rate of 0.00028 $^{\circ}C^{-1}$ and 0.0003 $^{\circ}C^{-1}$. It can be concluded that, at higher temperatures, T_{MTC} has a greater effect on COP, but after the critical temperature (−15 °C), its effect on exergy efficiency is marginally greater. Additionally, T_{LTC} has a substantially larger influence on system performance than T_{MTC}.

6.5. Effect of cascade condenser temperature difference

The variations of the TCRS' COP, compressor work, W_{total}, exergy efficiency, η and exergy destruction, $E_{D,total}$ with cascade condenser temperature difference, ΔT ranging from 4 °C to 8.5 °C are depicted in Fig. 12. It can be observed that with ΔT increases, both total compressor work and total exergy destruction increase linearly while a linear decrease is observed for *COP* and exergy efficiency. The reason for this trend is that as ΔT increases, both the MTCC and HTCC pressure ratio increase and thus cause an

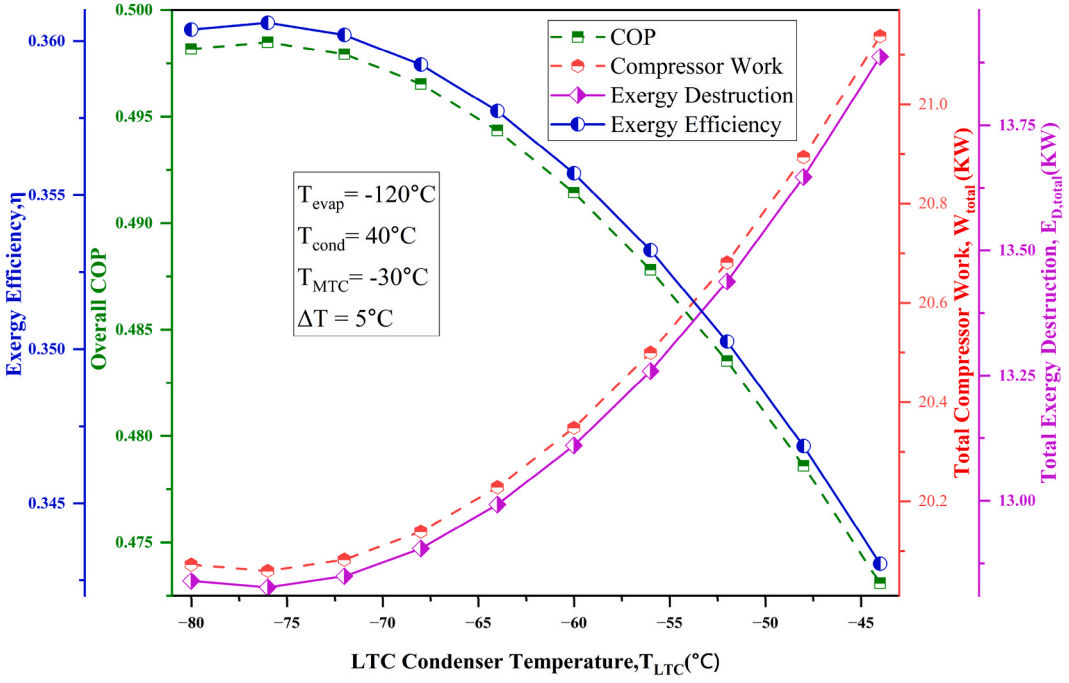

Fig. 10. Variations of Energy (COP, W_{total}) & Exergy (η, $E_{D,total}$) related parameters with T_{LTC}.

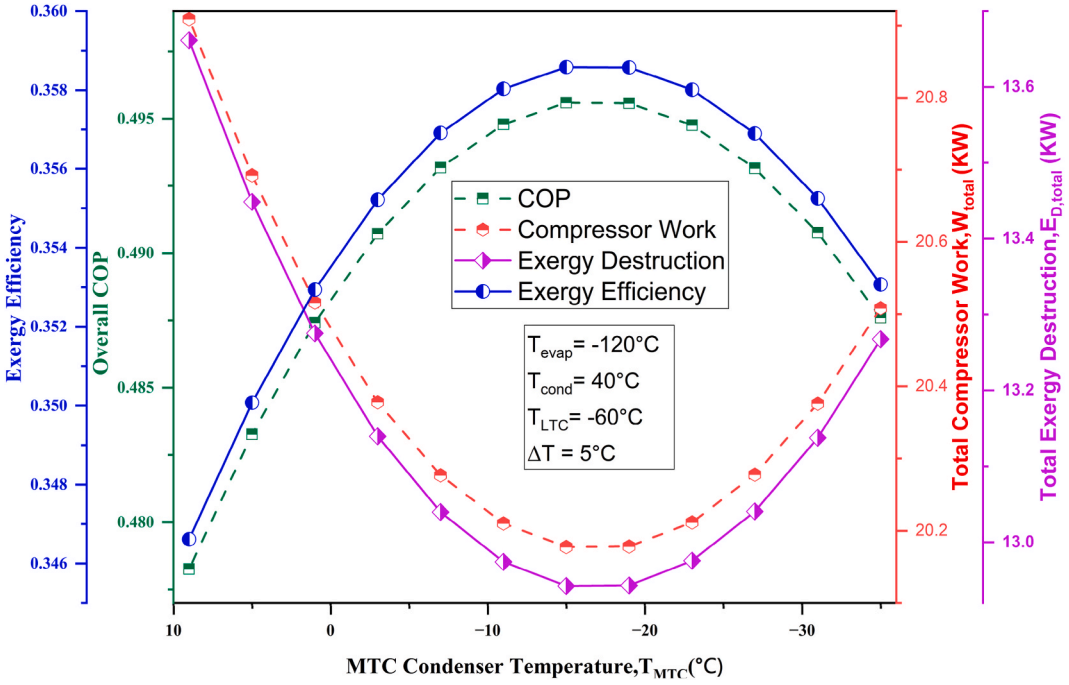

Fig. 11. Variations of Energy (COP, W_{total}) & Exergy (η, $E_{D,total}$) related parameters with T_{MTC}.

increased power requirement for both MTCC and HTCC while LTCC remains unaffected. For a 4.5 °C change in ΔT, compressor work and exergy destruction increase by 9.6 % and 15.2 %, respectively, resulting in a 9.6 % and 9.5 % decrease in COP and exergy efficiency, respectively. It is evident that, ΔT has marginally greater impact on COP (0.01 $^{\circ}C^{-1}$) than exergy efficiency (0.008 $^{\circ}C^{-1}$). Moreover, it has proven to be the most influential variable in this study.

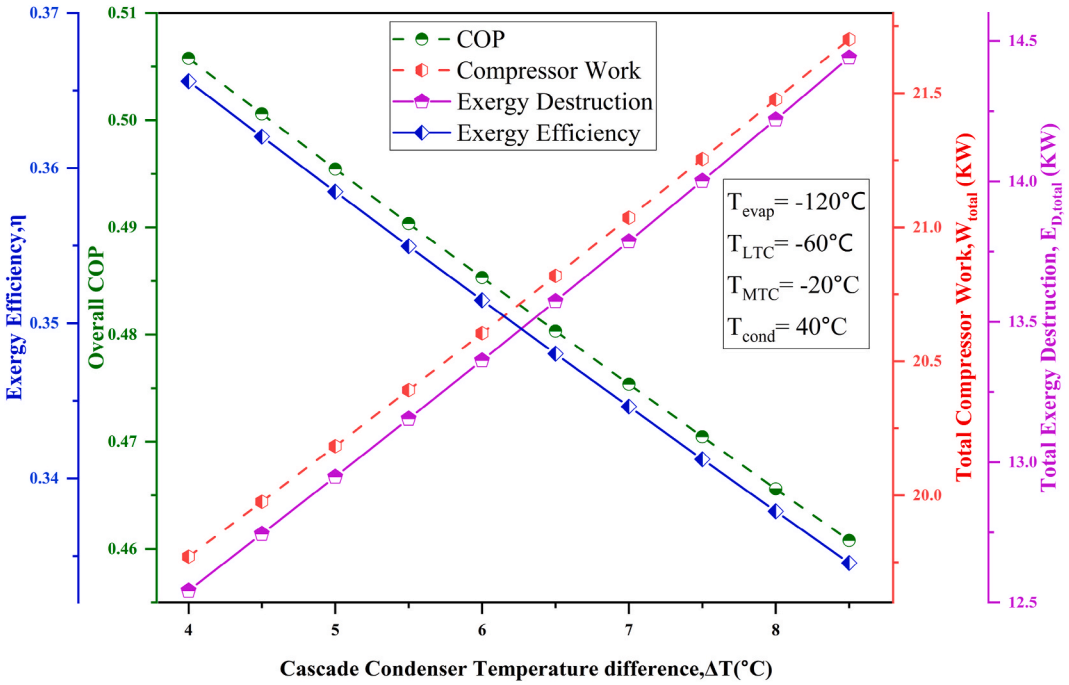

Fig. 12. Variations of Energy (COP, Wtotal) & Exergy (η, ED, total) related parameters with ΔT.

6.6. Effect of evaporator temperature on plant economics

The changes in total plant cost rate, individual cost rates, and equivalent CO_2 emission with evaporator temperature, T_{evap} ranging from −140 °C to −100.5 °C are illustrated in Fig. 13 while keeping T_{LTC}, T_{MTC}, T_{cond}, ΔT fixed at −70 °C, −30 °C, 40 °C, 5 °C respectively. It has been noticed that the overall plant cost rate shows a quadratic decrement initially with T_{evap}, reaching a minimum value at −107.5 °C, after that, increases rapidly while equivalent CO_2 emission keeps decreasing throughout this range. Examining the trends of individual cost rates can unveil the fundamental reasons for the trend of overall plant cost rates. An increase in T_{evap} drops the compressor power requirement and consequently, total operational and environmental impact costs will be reduced. But this will increase the evaporator heat transfer area which has a significant contribution to the total capital and maintenance (C&M) cost. Initially, the reduction of the compressor power causes total C&M cost to decrease, but after a certain temperature level, the cost related to the evaporator surpasses other contributors, and the overall C&M cost starts increasing sharply. Although operational and environmental penalty costs keep decreasing, the drastic increase in C&M costs causes the total plant cost to increase rapidly. Total plant cost and equivalent CO_2 emission initially decreases at an avg rate of 383 ($/year)/ °C and 1649.2 kg/ °C respectively to a minimum of 32500 $/year and 68160 kg respectively at −107.5 °C. Total CO_2 emission keeps a steady fall and reaches 60824 kg while the total plant cost rate's sudden rise (1158.9 ($/year)/ °C avg.) takes it to 40612 $/year at −100.5 °C. As a drastic increase in plant cost rate is observed after −107.5 °C, the operating temperature should be kept below this for economical operation.

6.7. Effect of condenser temperature on plant economics

Fig. 14 demonstrates the variations in total plant cost rates, individual cost rates, and equivalent CO_2 emission with condenser temperature, T_{cond} ranging from −140 °C to −100.5 °C. It is observed that the overall plant cost rate decreases initially for a specific temperature range (36 °C to 44 °C), afterward it starts increasing with T_{cond} while total equivalent CO_2 emission keeps increasing throughout this range. When T_{cond} increases, the total power requirement in HTCC increases which results in increased operational and environmental penalty costs, but C&M cost gets reduced as the condenser heat transfer area drops. Initially, the amount of increment in operational and environmental cost is less than the drop in C&M cost and so, the plant cost gets reduced till $T_{cond} = 44$ °C. After that, the increased amount in operational and maintenance cost becomes greater than the fall in C&M cost which eventually causes the plant cost to increase. Total plant cost decreases initially at an avg. rate of 270.9 ($/year)/ °C and reaches its optimum value (34810 $/year) at 44 °C. Then, it maintains a steady increase rate of 89.5 ($/year)/ °C until it reaches 36063 $/year at 58 °C. As the effect of T_{cond} on the cost rate of the plant is relatively insignificant, the optimal operational condition for this parameter, as determined by energy and exergy analysis, will prevail.

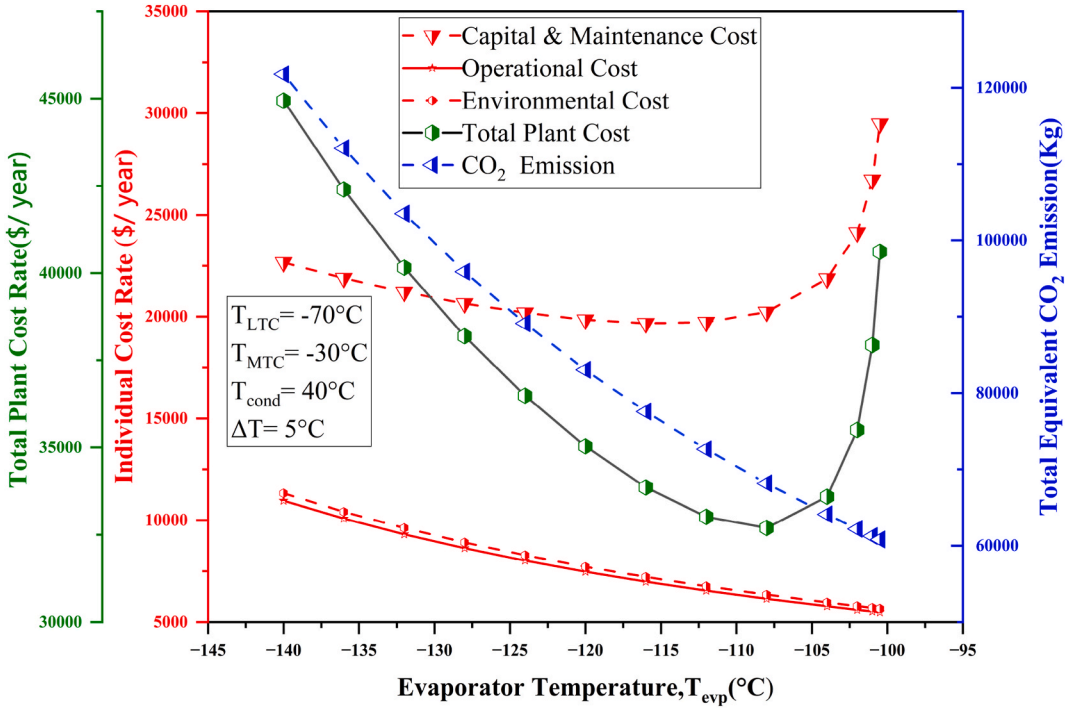

Fig. 13. Variations of plant cost rates and total CO2 emission with evaporator temperature, T_{evap}.

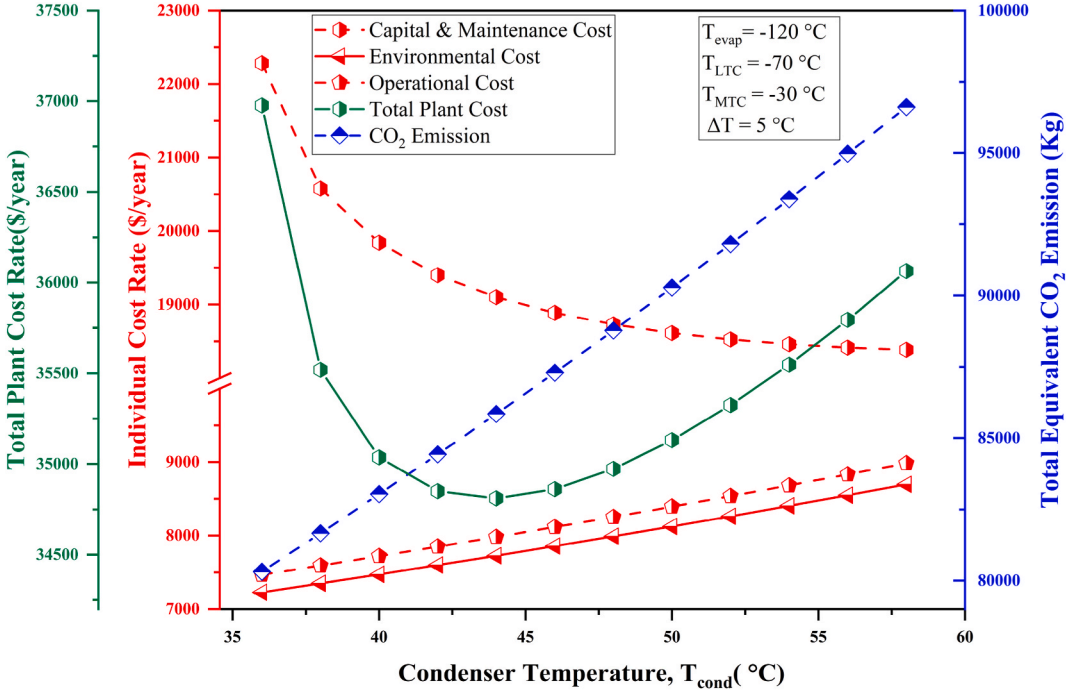

Fig. 14. Variations of plant cost rates and total CO2 emission with condenser temperature, T_{cond}.

6.8. *Effect of LTC condenser temperature on plant economics*

The variations in total plant cost rates, individual cost rates, and total equivalent CO_2 emission with LTC condenser temperature, T_{LTC} ranging from $-80\ ^{\circ}C$ to $-44\ ^{\circ}C$ are depicted in Fig. 15. It exhibits that the overall plant cost rate initially rises steadily with T_{LTC}, but a rapid increase occurs just after $-72.5\ ^{\circ}C$ whereas total CO_2 emission decreases initially up to a certain temperature range, after

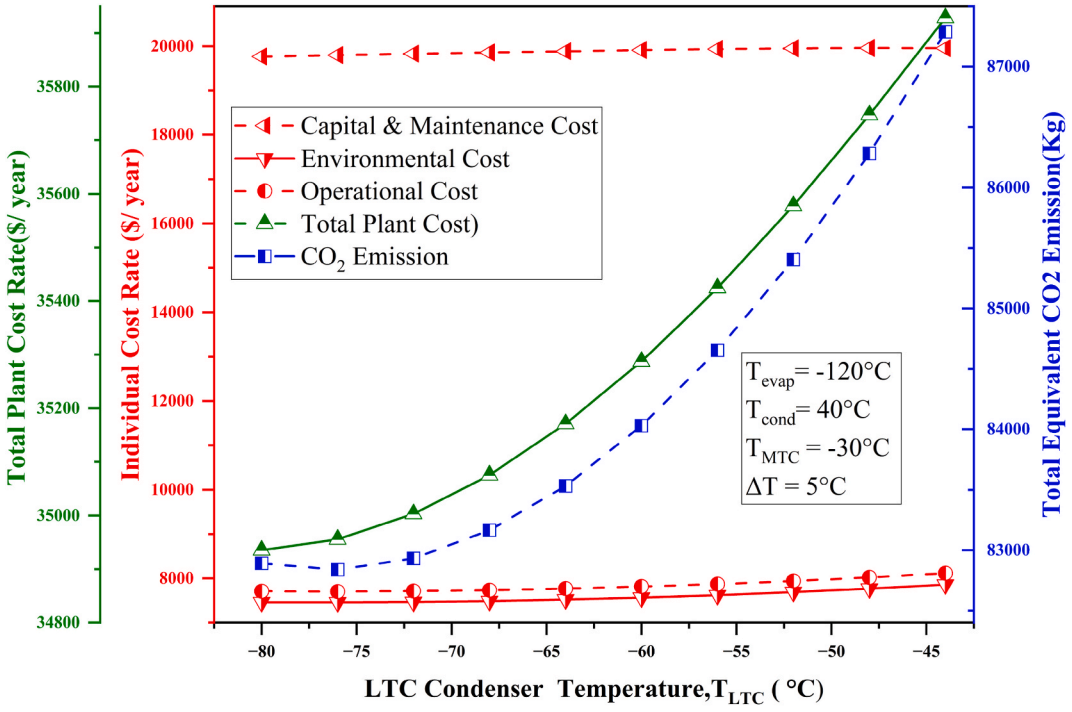

Fig. 15. Variations of plant cost rates and total CO2 emission with LTC condenser temperature, T_{LTC}.

that a drastic increase is noticed with LTC condenser temperature. This trend can be comprehended by scrutinizing individual cost rates. When T_{LTC} increases, the required power increases for LTCC but decreases for HTCC. This opposite behavior of overall input power will impact the operational cost and environmental impact cost. For a temperature range of $-80\ ^{\circ}C$ to $-76\ ^{\circ}C$, although total environmental cost and operational cost fall, the total plant cost rises very slowly because of the increase in its major contributor which is C&M cost. After that, all the contributors to the total plant cost increase with T_{LTC} and so, it starts increasing rapidly. At $-80\ ^{\circ}C$, the total plant cost rate is 34935.3 $/year which increases with an avg. rate of 5.2 ($/year)/ $^{\circ}C$ and rises to 34956 $/year at $-76\ ^{\circ}C$. After that with an avg. increase rate of 30.4 ($/year)/ $^{\circ}C$, total plant cost finally rises to 35928 $/year at $-44\ ^{\circ}C$.Clearly, T_{LTC} has little influence on the total plant cost rate compared to other parameters.

6.9. Effect of MTC condenser temperature on plant economics

Fig. 16 shows the changes in total plant cost rates, individual cost rates, and equivalent CO_2 emission with MTC condenser temperature, T_{MTC} ranging from $-35\ ^{\circ}C$ to $9\ ^{\circ}C$. It has been noticed that C & M cost increases with T_{MTC} whereas environmental and operational costs decrease initially for a temperature range of $-35\ ^{\circ}C$ to $-15\ ^{\circ}C$ and after that increase with T_{MTC}. These factors lead to a gradual increase in total plant cost until -15 °C, then it rises rapidly as all the individual cost rate increase for this range. The required power increases in MTCC and decreases in HTCC when T_{MTC} rises. These two opposing factors will determine the behavior of overall power requirement and subsequently total environmental cost and operational cost. Total plant cost increases at an avg. rate of 61.2 ($/year)/ $^{\circ}C$ up to $-15\ ^{\circ}C$, then it rises rapidly at an avg. rate of 482 ($/year)/ $^{\circ}C$, whereas CO_2 emission decreases at an avg. rate of 68.25 kg/ $^{\circ}C$ to reach its minimum value (83324 kg) at $-15\ ^{\circ}C$. After that it maintains an avg. increment rate of 125.8 kg/ $^{\circ}C$. Since T_{MTC} has a significant impact on plant economics, the optimum operating range should be below $-15\ ^{\circ}C$.

6.10. Effect of cascade condenser temperature difference on plant economics

The variations of total plant cost rates, individual cost rates, and equivalent CO_2 emission with cascade condenser temperature difference, ΔT ranging from 4 $^{\circ}C$ to 8.5 $^{\circ}C$ are depicted in Fig. 17. It demonstrates that both the overall plant cost rate and the equivalent CO_2 emission increase at constant rates with ΔT. Total plant cost rate rises from 35476 $/year at 4 $^{\circ}C$ to 37440 $/year at 8.5 $^{\circ}C$ at a constant rate of 418 ($/year)/ $^{\circ}C$ while total CO_2 emission rises from 81647 kg at 4 $^{\circ}C$ to 89616 kg at 8.5 $^{\circ}C$ at an avg. rate of 1700 kg/ $^{\circ}C$. The reason for this trend is that input power for MTCC and HTCC increases with ΔT, while it remains unaffected for LTCC. These factors lead to the gradual increase in all the individual costs and so, increase at a constant rate with ΔT is noticed for total plant cost rate. Evidently, ΔT has a strong influence on plant cost. However, since the optimal operating point (4 $^{\circ}C$) for ΔT is similar from both thermodynamic and economic point of view, this parameter can be excluded from the optimization task.

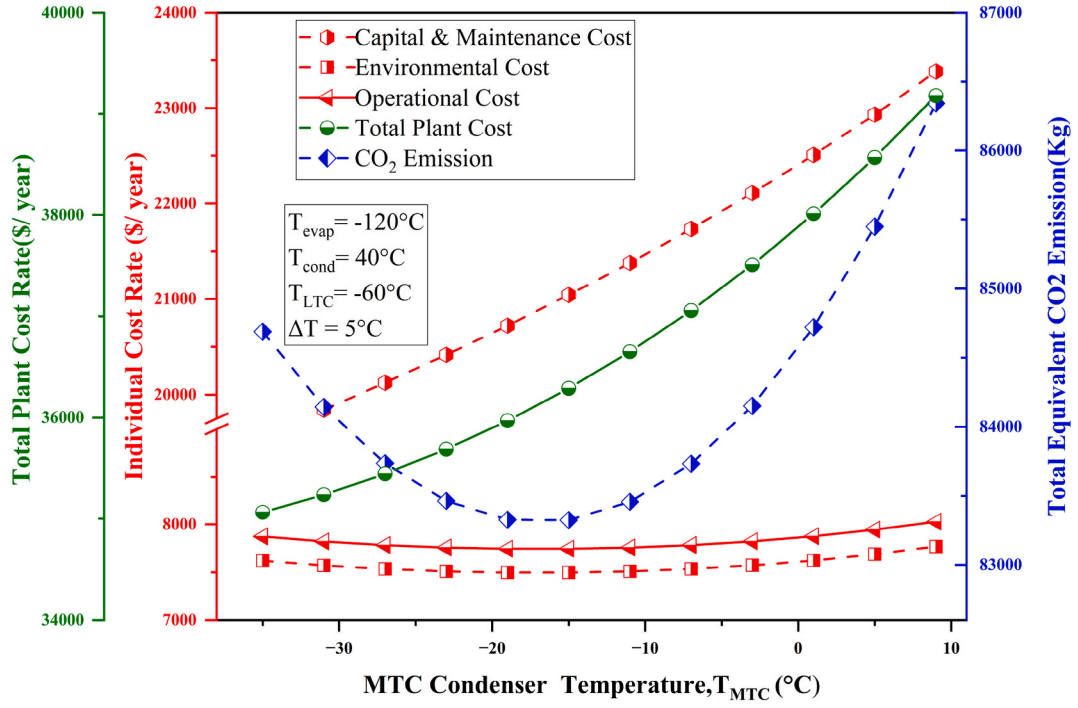

Fig. 16. Variations of plant cost rates and total CO2 emission with MTC condenser temperature, T_{MTC}.

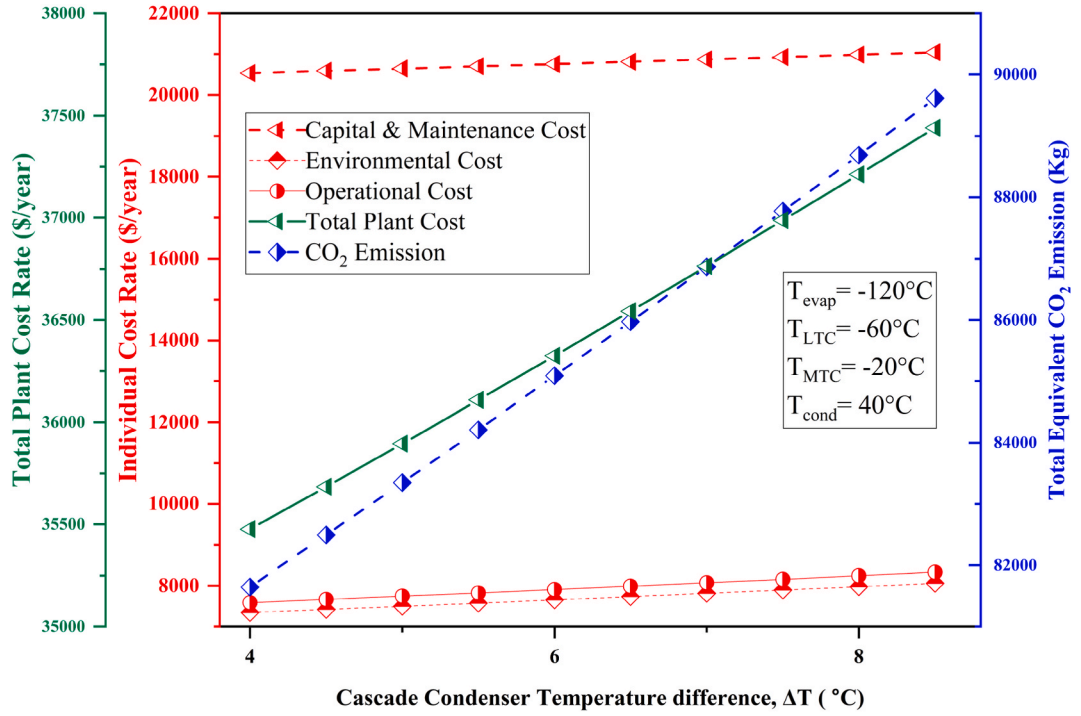

Fig. 17. Variations of plant cost rates and total CO2 emission with cascade condenser temperature, ΔT.

6.11. *Effect of both evaporator temperature and condenser temperature on plant economics*

The changes of overall plant cost with respect to both condenser temperature, T_{cond} and evaporator temperature, $T_{evap,}$ ranging from 36 °C to 61 °C and −140 °C to −101 °C respectively are presented in Fig. 18. It has been observed that the range of T_{evap} should be between −106 °C and −112 °C and T_{cond} range should be between 40 °C and 50 °C for the minimization of the plant cost rate. The minimum value of the plant cost rate is 32498 $/year which is obtained for $T_{evap} = -108$ °C and $T_{cond} = 44$ °C. The optimal range for the overall plant cost, however, may shift depending on the other operational parameters.

6.12. *Effect of both LTC & MTC condenser temperature on plant economics*

Fig. 19 demonstrates the variations in overall plant cost with LTC condenser temperature, T_{LTC} ranging from −80 °C to −35 °C and MTC condenser temperature, T_{MTC} ranging from −35 °C to 11 °C while keeping T_{evap}, T_{cond}, ΔT fixed at −120 °C, 40 °C and 5 °C respectively. The overall plant cost decreases with the decrease of both T_{LTC} and T_{MTC}. Therefore, the optimal temperature for minimizing total plant cost would be the temperature with the lowest values in the LTC and MTC condenser temperature ranges. At this operating condition, the minimum total plant cost rate is 34643 $/year which is obtained for LTC and MTC condenser temperatures at −80 °C and −35 °C respectively. However, this optimum range is only applicable for the operating conditions considered, but the trend should remain the same for other operating conditions as well.

6.13. *Pareto Analysis to determine the most impactful input parameters*

A sensitivity analysis has been conducted to evaluate the impact of input parameters on the three objective functions (Total Plant Cost, COP, and Exergy Efficiency). The dataset has been systematically varied across input parameters (T_{evap}, T_{LTC}, T_{MTC}, T_{cond} and ΔT) to observe corresponding changes in output parameters. This dataset has been utilized to generate a correlation matrix for both input and output parameters. Subsequently, Pareto Analysis has been employed to identify the most impactful (20 % input that causes 80 % outputs) input parameters in this study. Fig. 20 (a), (b), and (c) depict the correlation between input and output parameters for Total Plant Cost, COP, and exergy efficiency, respectively, while Fig. 20 (d), (e), and (f) illustrate Pareto Analysis for the corresponding outputs. The heatmap of the correlation matrix justifies the selection of input parameters, revealing significant correlations with the outputs. The Pareto Analysis results demonstrate that T_{evap} and ΔT are crucial factors for Total Plant Cost, while T_{evap} and T_{cond} are vital for both COP and exergy efficiency.

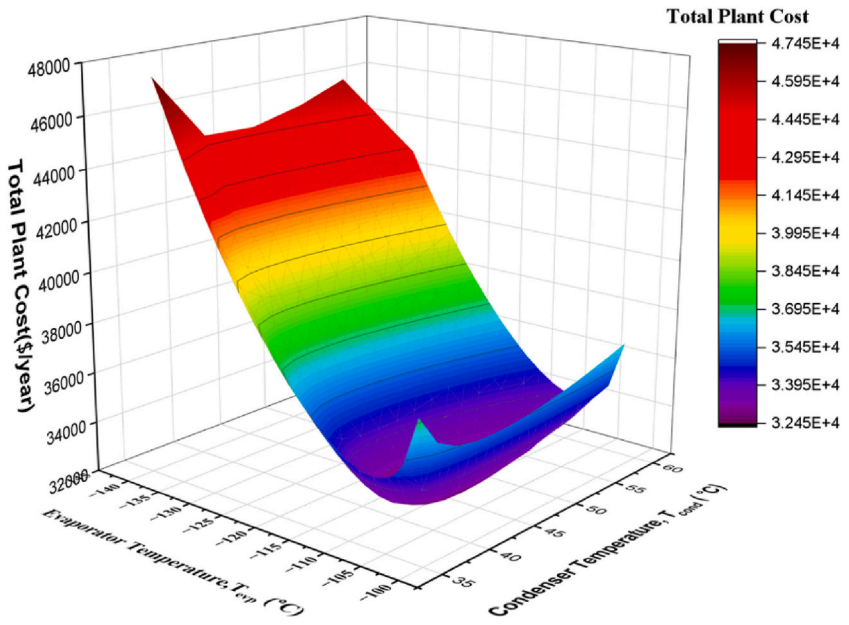

Fig. 18. Variations of plant cost rate with T_{cond} and T_{evap}.

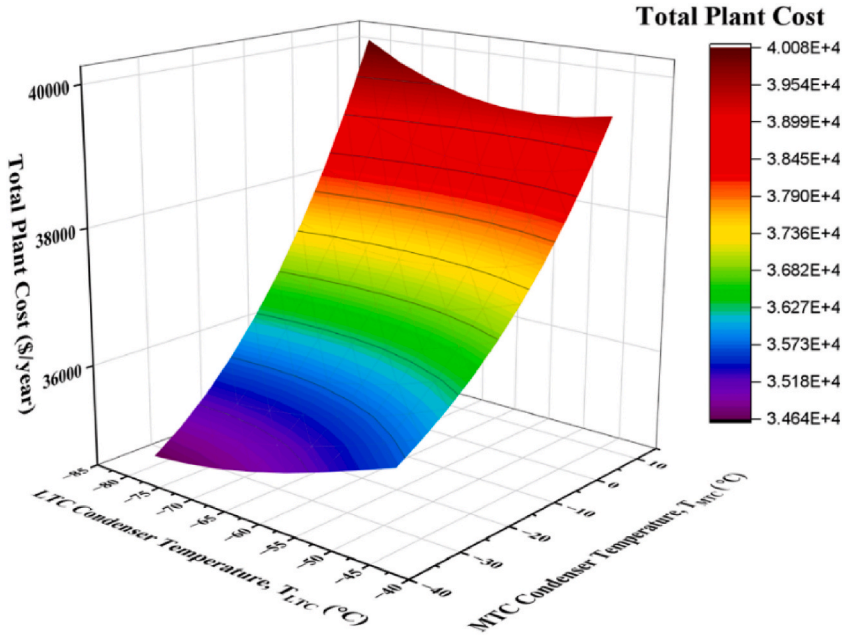

Fig. 19. Variations of total plant cost rate with T_{LTC} and T_{MTC}.

7. Multi objective optimization

7.1. Box-Behnken method for objective function generation

The quadratic equations for the three objective functions which are generated using Minitab software are given below. Cascade temperature difference, ΔT is not included as a contributing factor in the RSM method as it is evident after the parametric analysis part that, both exergy efficiency and COP will be maximum and total plant cost rate will be minimum at the lowest value of ΔT. Thus, ΔT has been kept at 4 °*C* to evade the unnecessary complexity of optimization procedure.

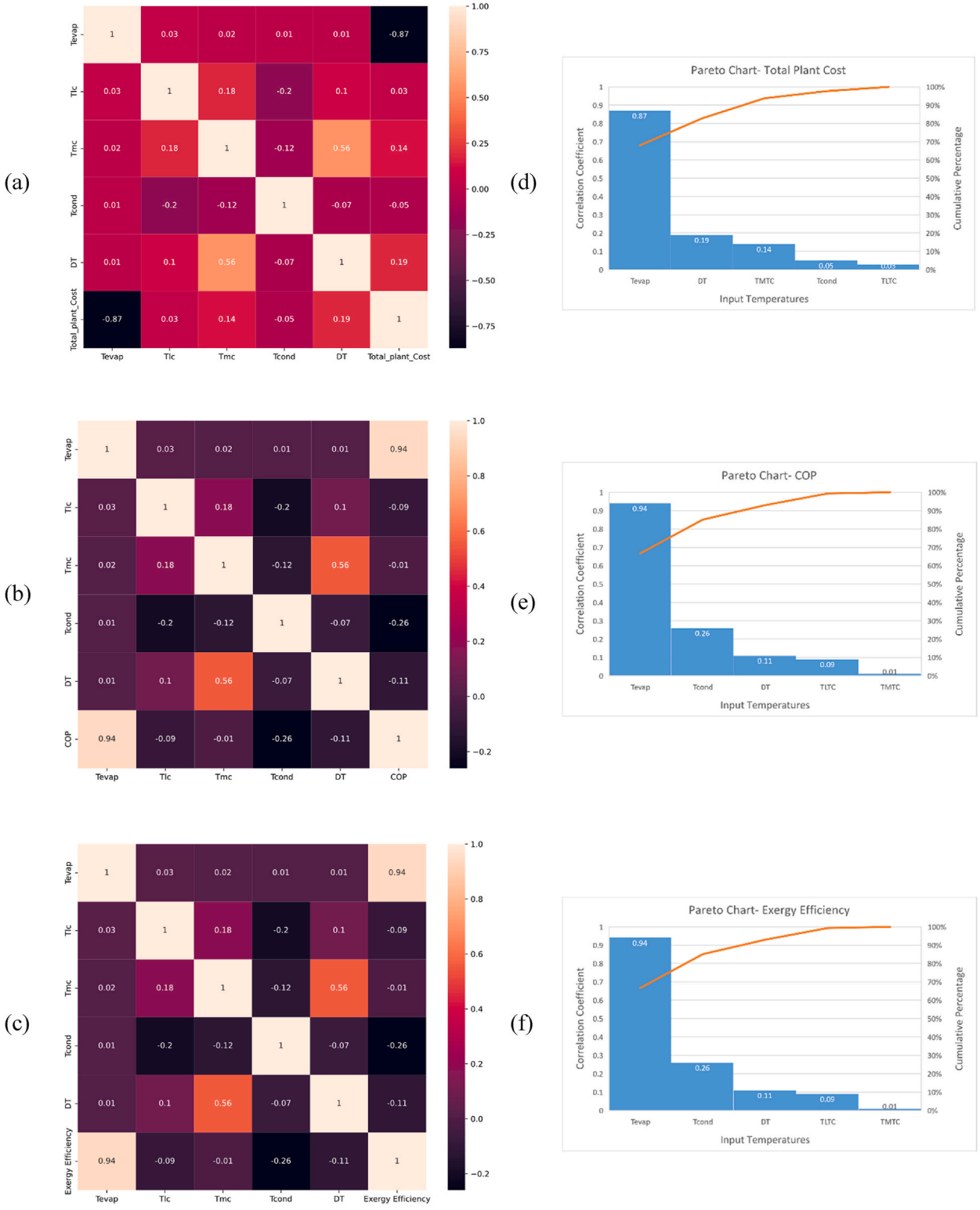

Fig. 20. Heatmap of the correlation coefficient matrix (a)–(c) and Pareto analysis (d)–(f) for the three objective functions (Total Plant Cost, COP, and exergy efficiency).

$$\begin{aligned}\textit{Total Plant Cost} = {} & 286832 + 3631.13 \times - 91.24 \times T_{LTC} + 287.10 \times T_{MTC} \\ & - 1735.7 \times T_{cond} + 16.6106 \times (T_{evap})^2 + 0.6317 \times (T_{LTC})^2 + 1.1752 \times (T_{MTC})^2 + 17.5936 \times (T_{cond})^2 - 1.4965 \times (T_{evap} \times T_{LTC}) \\ & - 0.5632 \times (T_{evap} \times T_{MTC}) + 1.4065 \times (T_{evap} \times T_{cond}) - 0.8651 (T_{LTC} \times T_{MTC}) - 6.3309 \times (T_{MTC} \times T_{cond})\end{aligned}$$

$$\begin{aligned}\textit{Exergy Efficiency} = {} & 1.93134 + 0.015717 \times \text{Tevap} - 0.000109 \times T_{LTC} - 0.000223 \times T_{MTC} \\ & - 0.010408 \times T_{cond} + 0.000026 \times (T_{evap})^2 - 0.000016 \times (T_{LTC})^2 \\ & - 0.000017 \times (T_{MTC})^2 + 0.000010 \times (T_{cond})^2 + 0.000016 \times (T_{evap} \times T_{LTC}) - 0.000002 \times (T_{evap} \times T_{MTC}) \\ & - 0.000060 \times (T_{evap} \times T_{cond}) + 0.000018 \times (T_{LTC} \times T_{MTC}) + 0.000003 \times (T_{LTC} \times T_{cond}) + 0.000013 \times (T_{MTC} \times T_{cond})\end{aligned}$$

$$\begin{aligned}COP = {} & 2.77349 + 0.022764 \times \text{Tevap} - 0.000158 \times T_{LTC} - 0.000322 \times T_{MTC} - 0.015075 \times T_{cond} + 0.000037 \times (T_{evap})^2 \\ & - 0.000024 \times (T_{LTC})^2 - 0.000024 \times (T_{MTC})^2 + 0.000015 \times (T_{cond})^2 + 0.000023 \times (T_{evap} \times T_{LTC}) - 0.000002 \times (T_{evap} \times T_{MTC}) \\ & - 0.000087 \times (T_{evap} \times T_{cond}) + 0.000026 \times (T_{LTC} \times T_{MTC}) + 0.000004 \times (T_{LTC} \times T_{cond}) + 0.000019 \times (T_{MTC} \times T_{cond})\end{aligned}$$

7.1.1. Accuracy of the quadratic equations

To assess the accuracy of the quadratic equations derived through the Box-Behnken method, a dataset was systematically generated across a specified range: ($T_{evap} = -140$ to $-110\ ^\circ C$) , ($T_{cond} = 36$ to $57\ ^\circ C$), ($T_{LTC} = -80$ to $-72\ ^\circ C$) and ($T_{MTC} = -35$ to $7\ ^\circ C$). A subset of this dataset is presented in Table 16 for reference. The accuracy of the quadratic equations was then rigorously evaluated using various error metrics, as delineated in Table 17. It can be observed that MAE, MAPE and RMSE values are within the expected range for all three output functions. Furthermore, the R^2 values, approaching unity, affirm a close alignment between the quadratic equations and the underlying model. This convergence strongly suggests that the equations aptly capture the intricacies of the model, substantiating their appropriateness for predictive purposes.

7.2. Pareto Front for three objective functions

The optimum solutions of the three objective functions which are generated by using *gamultiobj* solver in MATLAB optimization toolbox are presented in Fig. 21. It is evident that a rise in *COP* and exergy efficiency causes total plant cost to increase. Total plant cost rate increases from 33295 $/year to 40639 $/year for 38.1 % increase in exergy efficiency (from 0.37 to 0.511) and 39.2 % increase in COP (from 0.51 to 0.71).

7.3. Optimum solutions from decision making techniques

Although all the solutions of the Pareto front are optimum, a unique solution has been extracted from the Pareto Front by employing decision making techniques (TOPSIS & LINMAP) to analyze the TCR system comprehensively. Fig. 22 depicts the optimum point after employing TOPSIS and LINMAP, it is also listed in Table 18. It has been found that both decision-making techniques derive the same unique solution. The thermodynamic properties of each state point and the performance of the TCRS have been determined at the optimum point and are listed in Table 19 and Table 20 respectively. Three objective functions in this work, total plant cost rate, exergy efficiency, and COP, are 38262.05 $/year, 0.51 and 0.71 respectively at optimum point.

Table 16
Sample dataset to compare the actual and predicted value.

Tevap ($^\circ C$)	T_{LTC} ($^\circ C$)	T_{MTC} ($^\circ C$)	T_{cond} ($^\circ C$)	ΔT ($^\circ C$)	Plant Cost Actual	Plant Cost Predicted	Exergy Efficiency Actual	Exergy Efficiency Predicted	COP Actual	COP Predicted
−113	−72	7	57	4	35196.12	35873.75	0.35	0.35	0.48	0.47
−116	−72	7	57	4	35913.04	35839.91	0.33	0.34	0.46	0.45
−119	−72	7	57	4	36820.87	36105.07	0.32	0.32	0.44	0.43
−137	−76	7	57	4	45573.1	43917.87	0.23	0.24	0.32	0.31
−113	−72	4	57	4	34949.81	35678.46	0.35	0.35	0.49	0.48
−140	−72	7	57	4	47549.9	46332.89	0.22	0.23	0.3	0.29
−113	−74	7	57	4	35270.7	35914.59	0.35	0.35	0.48	0.47
−116	−74	7	57	4	35983.1	35871.77	0.33	0.33	0.46	0.45
−119	−74	7	57	4	36885.8	36127.95	0.32	0.32	0.44	0.43
−122	−74	7	57	4	37949.7	36683.11	0.3	0.3	0.41	0.4
−134	−78	7	45	4	43898.25	43952.1	0.27	0.27	0.36	0.35
−140	−74	7	57	4	47563.94	46292.92	0.22	0.23	0.3	0.29
−119	−78	−14	51	4	34997.91	34572.13	0.34	0.34	0.47	0.46
−116	−76	7	57	4	36062.78	35908.68	0.33	0.33	0.45	0.45
−119	−76	7	57	4	36960.58	36155.88	0.32	0.32	0.43	0.42

Table 17
Accuracy of the quadratic equations based on some error metrics.

Outputs	MAE	MAPE	RMSE	R^2 Score
Total Plant Cost	754.27	0.0191	871.46	0.96
COP	0.0088	0.0215	0.009	0.98
Exergy Efficiency	0.0026	0.0091	0.003	0.995

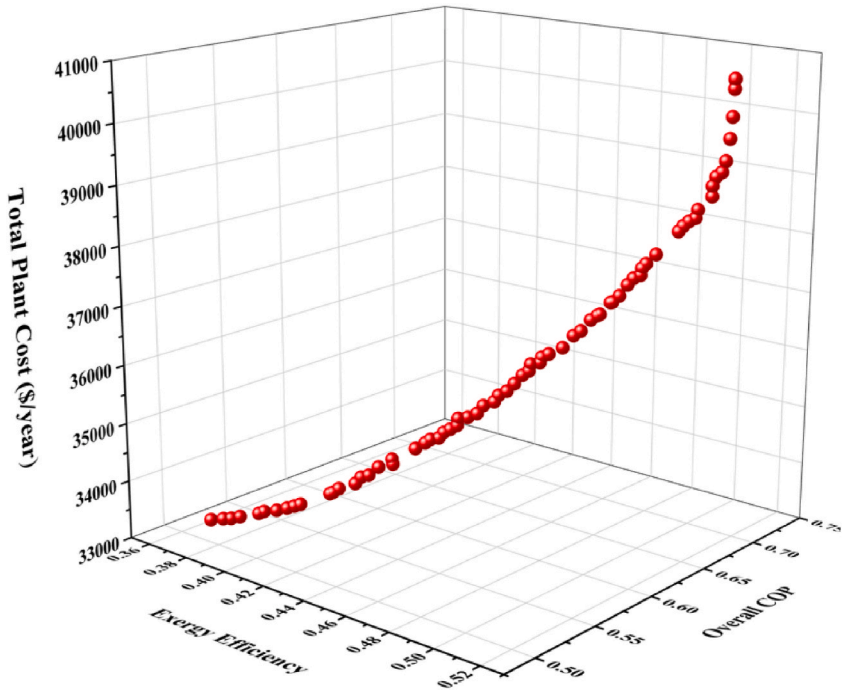

Fig. 21. Pareto front for the triple objective optimization of the TCRS.

7.4. Exergy destruction at the optimum point

To investigate the TCR system comprehensively, exergy destruction across each of the components at the optimum point has been determined and further depicted in Fig. 23. It has been noticed that HTC compressor (19.3 %) and HTC throttle valve (15.5 %) cause the majority (35 %) of the total exergy destruction and to improve the total exergy efficiency, these parts should be given the most attention. Condenser (11.7 %), MTC compressor (11.2 %), CHX1 (10 %), LTC compressor (9 %), evaporator (8.4 %), CHX2 (6.6 %) are next to this list according to their contribution to total exergy destruction rate and there is room for improvements in these components as well. As the LTC throttle (3.1 %) and MTC throttle (5.1 %) have insignificant impact on total exergy destruction, improvement for these components can be avoided to reduce overall plant cost.

7.5. Energy flow at the optimum point

The energy flow across each of the components of the TCRS at the optimum operating condition has been depicted in Fig. 24 For a refrigeration system with a capacity of 10 kW, it is observed that the total work input necessary is 14.1 kW. Furthermore, approximately 57 % of the total work input has to be provided to the high-temperature circuit (HTC) compressor.

7.6. Plant economics at the optimum point

Fig. 25 illustrates the various cost parameters (capital & maintenance cost, operational cost, environmental cost) of the TCRS at the optimum operating condition. It can be observed that the majority (72 %) of the cost is related to the capital investment and maintenance cost while environmental and operational costs comprise 14 % each of the total cost. The preeminent contributors to the total capital and maintenance cost are the evaporator (43 %) and condenser (20 %). This underscores the necessity to prioritize efforts aimed at cost reduction for these components.

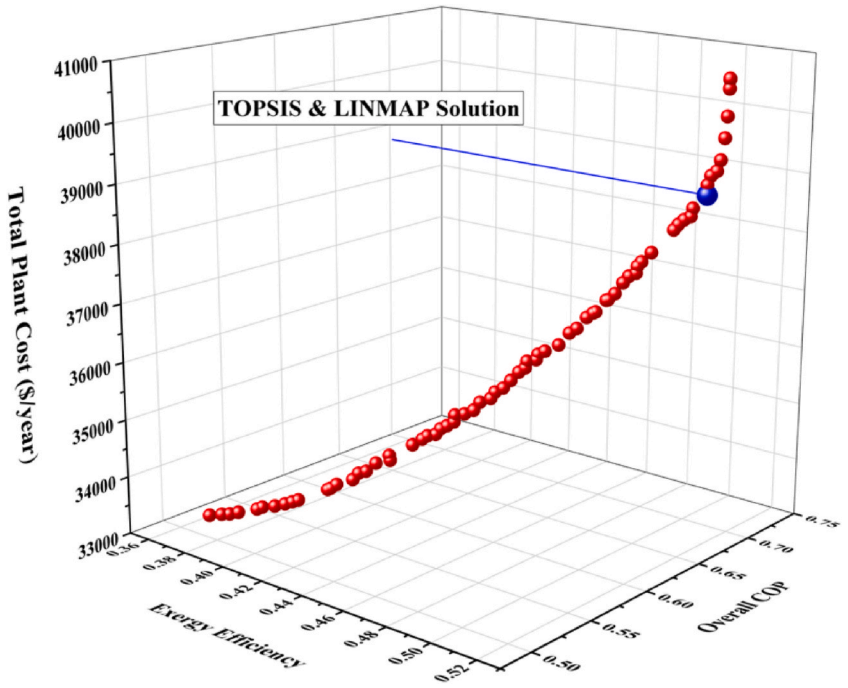

Fig. 22. Unique solution on Pareto Front after employing decision making techniques.

Table 18
Optimized point for each decision-making technique.

T_{evap}	T_{LTC}	T_{MTC}	T_{cond}	Decision making Technique
−101.023	−69.047	−34.651	36.545	TOPSIS
−101.023	−69.047	−34.651	36.545	LINMAP

Table 19
Thermodynamic properties of each state point at optimum operating condition.

State Point	Fluid	T (°C)	P (kPa)	$\dot{m}$ (kg/s)	h (kJ/kg)	s (kJ/kg/k)	$\dot{E}$ (kW)
1	1-Butene	−101.02	0.209	0.02	282.46	1.87	−5.51
2	1-Butene	−10.90	3.574	0.02	391.80	1.96	−3.48
3	1-Butene	−69.05	3.574	0.02	−129.41	−0.55	2.03
4	1-Butene	−101.02	0.209	0.02	−129.41	−0.52	1.81
5	Heptane	−73.05	0.002	0.04	47.66	0.79	−6.04
6	Heptane	−4.83	0.123	0.04	142.81	0.86	−3.39
7	Heptane	−34.65	0.123	0.04	−303.38	−1.00	0.52
8	Heptane	−73.05	0.002	0.04	−303.38	−0.97	0.16
9	m-xylene	−38.65	0.008	0.05	117.50	0.87	−5.43
10	m-xylene	92.98	2.116	0.05	274.23	0.95	1.22
11	m-xylene	36.55	2.116	0.05	−197.71	−0.55	0.01
12	m-xylene	−38.65	0.008	0.05	−197.71	−0.48	−1.07
13	Air	−90.00	101.300	2.39	308.74	3.39	30.23
14	Air	−100.00	101.300	2.39	298.65	3.33	36.97
15	Air	25.00	101.300	0.99	424.44	3.88	0.00
16	Air	35.00	101.300	0.99	434.50	3.91	0.40

8. Conclusion

A comprehensive analysis based on thermodynamic, economic, and environmental perspectives of a 10 kW TCR system installed with hydrocarbon refrigerants (1-butene/Heptane/m-Xylene) has been conducted in this work. A sensitivity analysis has been employed to comprehend the effect of different operational parameters on the system performance. In addition, multi-objective (COP, exergy efficiency, overall plant cost) optimization using genetic algorithm and subsequent decision techniques (TOPSIS & LINMAP) have been employed to derive the optimum operating point. Furthermore, system performance, energy flow, exergy destruction and

Table 20
TCR system performance at optimum point.

Parameters	Value
Total compressor work	14.08 kW
Total exergy destruction	6.95 kW
LTC COP	3.77
MTC COP	3.69
HTC COP	2.01
Overall COP	0.71
Exergy Efficiency	0.51
Capital and maintenance cost	27621.49 $/year
Operational cost	5406.79 $/year
Total equivalent CO_2 emission	58153.03 kg
CO_2 penalty cost	5233.77 $/year
Total plant cost	38262.05 $/year

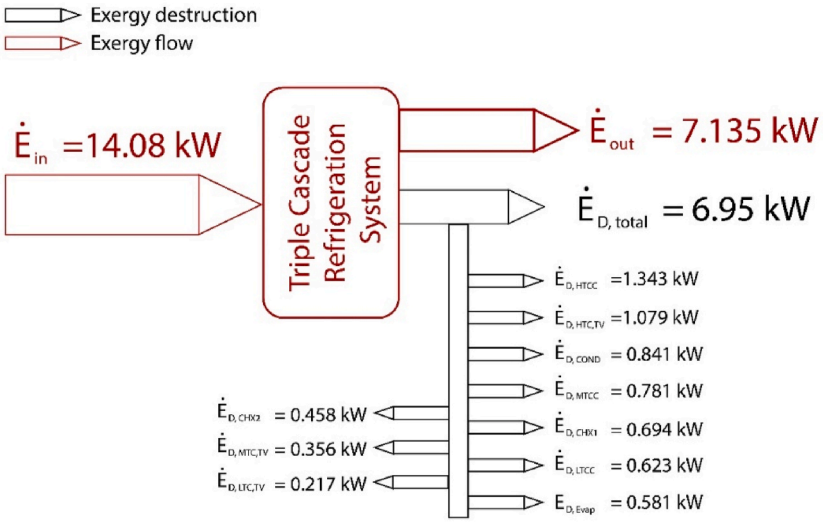

Fig. 23. Exergy destruction across each of the components at optimum point.

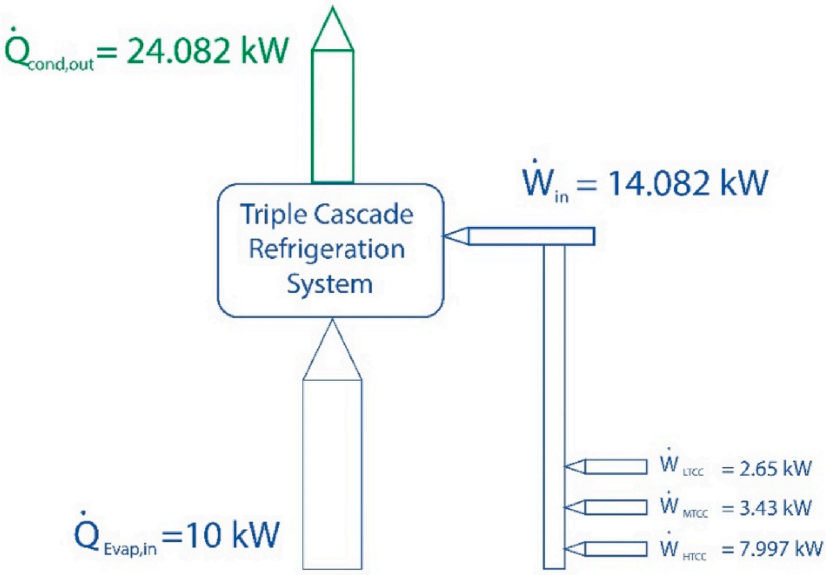

Fig. 24. Energy flow across various components of the TCRS at optimum point.

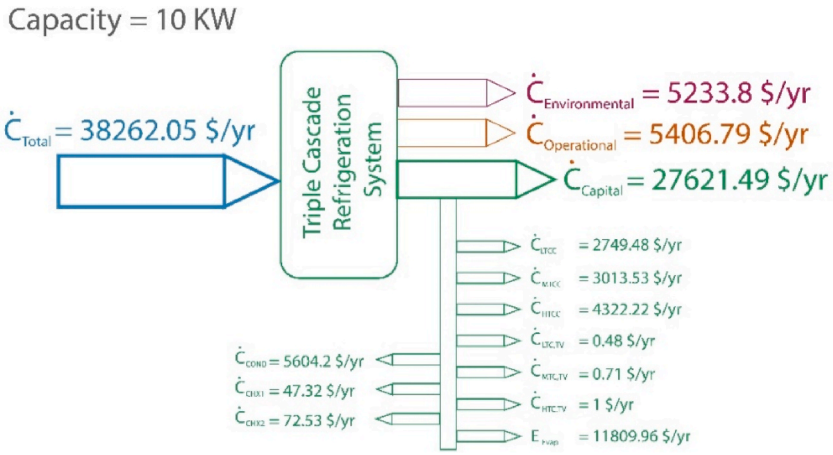

Fig. 25. Various cost parameters of the TCRS at optimum point.

cost rate for each of the components have been evaluated at optimum point to make a priority-based improvement. This investigation allows us to derive the following findings:

- Both COP and exergy efficiency increases with evaporator temperature, T_{evap} (91.2 % & 83.7 % increment respectively for temperature range $-140\ ^{\circ}C$ to $-104\ ^{\circ}C$) while overall plant cost rate shows a quadratic decrement (383 ($/year)/$^{\circ}C^{-1}$) initially, reaching a minimum value of 32500 $/year at -107.5 °C, after that, increases rapidly (1158.9 ($/year)/$^{\circ}C^{-1}$).
- The system performance (COP and exergy efficiency) deteriorates with condenser temperature (15.7 % & 16.2 % decrement respectively for temperature range $36\ ^{\circ}C$ to $58\ ^{\circ}C$) while the overall plant cost rate decreases (270.9 ($/year)/$^{\circ}C^{-1}$) initially, reaching a minimum value of 34810 $/year at 44 °C and afterward it starts increasing (89.5 ($/year)/$^{\circ}C^{-1}$).
- With LTC condenser temperature, T_{LTC} both COP & exergy efficiency exhibits increment (0.0025 $^{\circ}C^{-1}$) initially, reaching maximum value (0.499 and 0.361 respectively) at $T_{LTC} = -76$ °C and after that, both parameters show quadratic decrement (0.0008 $^{\circ}C^{-1}$ and 0.0006 $^{\circ}C^{-1}$) while overall plant cost rate initially rises steadily with T_{LTC}, but a rapid increase occurs just after -72.5 °C.
- COP and exergy efficiency shows increment (0.00073 $^{\circ}C^{-1}$ and 0.0005 $^{\circ}C^{-1}$ respectively) initially with MTC condenser temperature, T_{MTC} and rise to their maximum value (0.5 and 0.36 respectively) at $T_{MTC} = -15$ °C, then both of these parameters start declining while gradual increase is observed in total plant cost until $T_{MTC} = -15$ °C, then it rises rapidly (482 ($/year)/$^{\circ}C^{-1}$).
- A linear decrease in COP & exergy efficiency (9.6 % and 9.5 % respectively) is noticed with cascade temperature difference ΔT ($4\ ^{\circ}C$ to $8.5\ ^{\circ}C$) while overall plant cost rate increases (418 ($/year)/$^{\circ}C^{-1}$) linearly. As all the functions are already optimized at the minimum temperature of ΔT , this parameter has been excluded from the optimization.
- Both TOPSIS & LINMAP gives identical solution and *COP*, exergy efficiency and overall cost rates are found 0.71, 0.51 and 38262.05 $/year respectively at optimum temperature ($T_{evap} = -101.023\ ^{\circ}C$, $T_{cond} = 36.545\ ^{\circ}C$, $T_{LTC} = -69.047\ ^{\circ}C$ and $T_{MTC} = -34.651\ ^{\circ}C$)
- Finally, exergy destruction at optimum condition shows that the focus should be on the improvement of HTC compressor and HTC throttle valve, a major contributor (35 %) to overall exergy destruction.

At the optimum point, the economic analysis reveals that capital and maintenance costs are the primary contributors, accounting for 72 %, with 63 % of this cost attributed to the evaporator and condenser components.

9. Limitations and future recommendations

This study, which relies on simulations for the TCRS, inherently recognizes the possibility of deviations in results when extending findings to real-world scenarios. The ensuing section encompasses a comprehensive discussion of the limitations associated with this study, accompanied by recommendations for future research within this sector.

9.1. Limitations

- As this is a simulation-based study of a TCRS, it is acknowledged that there may be deviations in the results when applied to real-life scenarios.
- The quadratic equations were derived through the Box-Behnken method, and subsequent optimization was carried out based on these equations. While the equations demonstrate a notable level of accuracy, it is recognized that they may not perfectly align with the actual model across all ranges of the input dataset.

- Design parameters, assumed or adopted from the literature review, may require adjustment based on specific application requirements and locations.
- The optimization process was conducted based on certain assumptions, recognizing that these assumptions may need to be revisited or adjusted in real-life applications.
- Conventional exergy analysis, while determining overall exergy destruction, lacks the ability to differentiate between endogenous and exogenous sources, limiting insights into specific components causing maximum exergy destruction.

9.2. Future recommendations

- An advanced exergy analysis might be performed on this cycle to get a detailed analysis of the components' contribution to the exergy destruction and an advanced exergo-economic analysis can be employed as well to unveil more detailed improvement potentials of the TCRS economics in the next work.
- Advanced multi-objective optimization algorithms, such as NSGA-III, SMPSO, and MOEAD, may be used. Machine learning models may be used to enhance the precision of regression models in addition to the Box Behnken approach.
- The simulation model will be compared to an experimental model to uncover significant opportunities for improvement.

Data availability statement

The authors have initially validated the code with a reference model. Subsequently, a dataset has been generated to train a regression model for further works in this paper. If this dataset proves beneficial for future endeavors in this sector, the authors will make it available on request.

Ethics statement

The study did not necessitate review and/or approval by an ethics committee, as it exclusively involves a software-based simulation of a triple cascade refrigeration system. The authors systematically developed a model, validated it against a reference model, and subsequently optimized the input parameters. Given the non-invasive nature of the study and the absence of involvement with human subjects, the need for informed consent was not required as well.

CRediT authorship contribution statement

Imrul Kayes: Writing – original draft, Visualization, Validation, Methodology, Investigation, Formal analysis, Conceptualization. **Raditun E. Ratul:** Writing – original draft, Methodology, Formal analysis, Conceptualization. **Abyaz Abid:** Writing – original draft, Methodology, Formal analysis, Conceptualization. **Fawaz Bukht Majmader:** Writing – original draft, Methodology, Formal analysis, Conceptualization. **Yasin Khan:** Writing – review & editing, Supervision, Formal analysis, Conceptualization. **M Monjurul Ehsan:** Writing – review & editing, Supervision, Formal analysis, Conceptualization.

Declaration of competing interest

The authors declare that they have no known competing financial interests or personal relationships that could have appeared to influence the work reported in this paper.

References

[1] J.-L. Dupont, The Role of Refrigeration in the Global Economy (2019), 38th Note on Refrigeration Technologies, 2019. https://iifir.org/en/fridoc/the-role-of-refrigeration-in-the-global-economy-2019-142028. (Accessed 26 December 2022).
[2] K. Harby, Hydrocarbons and their mixtures as alternatives to environmental unfriendly halogenated refrigerants: an updated overview, Renew. Sustain. Energy Rev. 73 (Jun. 2017) 1247–1264, https://doi.org/10.1016/j.rser.2017.02.039.
[3] A. Mota-Babiloni, J. Navarro-Esbrí, P. Makhnatch, F. Molés, Refrigerant R32 as lower GWP working fluid in residential air conditioning systems in Europe and the USA, Renew. Sustain. Energy Rev. 80 (Dec. 2017) 1031–1042, https://doi.org/10.1016/j.rser.2017.05.216.
[4] M.W. Faruque, Y. Khan, M.H. Nabil, M.M. Ehsan, Parametric analysis and optimization of a novel cascade compression-absorption refrigeration system integrated with a flash tank and a reheater, Results in Engineering 17 (Mar. 2023) 101008, https://doi.org/10.1016/j.rineng.2023.101008.
[5] Z. Wu, W. Ma, Z. Xian, Q. Liu, A. Hui, W. Zhang, The impact of quick-freezing methods on the quality, moisture distribution and microstructure of prepared ground pork during storage duration, Ultrason. Sonochem. 78 (Oct. 2021) 105707, https://doi.org/10.1016/j.ultsonch.2021.105707.
[6] S. Powell, A. Molinolo, E. Masmila, S. Kaushal, Real-Time temperature mapping in ultra-low freezers as a standard quality assessment, Biopreserv. Biobanking 17 (2) (Apr. 2019) 139–142, https://doi.org/10.1089/bio.2018.0108.
[7] I. Tolstorebrov, T.M. Eikevik, M. Bantle, Effect of low and ultra-low temperature applications during freezing and frozen storage on quality parameters for fish, Int. J. Refrig. 63 (Mar. 2016) 37–47, https://doi.org/10.1016/j.ijrefrig.2015.11.003.
[8] J. Zhang, H. Meerman, R. Benders, A. Faaij, Comprehensive review of current natural gas liquefaction processes on technical and economic performance, Appl. Therm. Eng. 166 (Feb. 2020) 114736, https://doi.org/10.1016/j.applthermaleng.2019.114736.
[9] R.E. Ratul, F. Ahmed, S. Alam, Md Rezwanul Karim, A.A. Bhuiyan, Numerical study of turbulent flow and heat transfer in a novel design of serpentine channel coupled with D-shaped jaggedness using hybrid nanofluid, Alex. Eng. J. 68 (Apr. 2023) 647–663, https://doi.org/10.1016/j.aej.2023.01.061.
[10] Z. Sun, Q. Wang, B. Dai, M. Wang, Z. Xie, Options of low Global Warming Potential refrigerant group for a three-stage cascade refrigeration system, Int. J. Refrig. 100 (2019) 471–483, https://doi.org/10.1016/j.ijrefrig.2018.12.019.
[11] R.G. Craig, H.J. Slesnick, F.A. Peyton, Application of 17-7 precipitation-hardenable stainless steel in dentistry, J. Dent. Res. 44 (3) (May 1965) 587–595, https://doi.org/10.1177/00220345650440032401.

[12] A.F. Santos, P.D. Gaspar, H.J.L. de Souza, Refrigeration of COVID-19 vaccines: ideal storage characteristics, energy efficiency and environmental impacts of various vaccine options, Energies 14 (7) (Mar. 2021) 1849, https://doi.org/10.3390/en14071849.
[13] M. Kanoglu, I. Dincer, M.A. Rosen, Performance analysis of gas liquefaction cycles, Int. J. Energy Res. 32 (1) (Jan. 2008) 35–43, https://doi.org/10.1002/er.1333.
[14] M. Walid Faruque, Y. Khan, M. Hafiz Nabil, M. Monjurul Ehsan, A. Karim, Thermal performance evaluation of a novel ejector-injection cascade refrigeration system, Therm. Sci. Eng. Prog. 39 (Mar. 2023) 101745, https://doi.org/10.1016/j.tsep.2023.101745.
[15] A. Mota-Babiloni, et al., Ultralow-temperature refrigeration systems: configurations and refrigerants to reduce the environmental impact, Int. J. Refrig. 111 (Mar. 2020) 147–158, https://doi.org/10.1016/j.ijrefrig.2019.11.016.
[16] R. Roy, B.K. Mandal, Energetic and exergetic performance comparison of cascade refrigeration system using R170-R161 and R41-R404A as refrigerant pairs, Heat Mass Tran. 55 (3) (Mar. 2019) 723–731, https://doi.org/10.1007/s00231-018-2455-7.
[17] M.W. Faruque, M.R. Uddin, S. Salehin, M.M. Ehsan, A comprehensive thermodynamic assessment of cascade refrigeration system utilizing low GWP hydrocarbon refrigerants, International Journal of Thermofluids 15 (Aug. 2022) 100177, https://doi.org/10.1016/j.ijft.2022.100177.
[18] Y. Khan, M.W. Faruque, M.H. Nabil, M.M. Ehsan, Ejector and vapor injection enhanced novel compression-absorption cascade refrigeration systems: a thermodynamic parametric and refrigerant analysis, Energy Convers. Manag. 289 (Aug. 2023) 117190, https://doi.org/10.1016/j.enconman.2023.117190.
[19] O. Rezayan, A. Behbahaninia, Thermoeconomic optimization and exergy analysis of CO2/NH3 cascade refrigeration systems, Energy 36 (2) (Feb. 2011) 888–895, https://doi.org/10.1016/j.energy.2010.12.022.
[20] M. Mafi, S.M.M. Naeynian, M. Amidpour, Exergy analysis of multistage cascade low temperature refrigeration systems used in olefin plants, Int. J. Refrig. 32 (2) (Mar. 2009) 279–294, https://doi.org/10.1016/j.ijrefrig.2008.05.008.
[21] Z. Sun, et al., Comparative analysis of thermodynamic performance of a cascade refrigeration system for refrigerant couples R41/R404A and R23/R404A, Appl. Energy 184 (Dec. 2016) 19–25, https://doi.org/10.1016/j.apenergy.2016.10.014.
[22] S. Saleh, V. Pirouzfar, A. Alihosseini, Performance analysis and development of a refrigeration cycle through various environmentally friendly refrigerants, J. Therm. Anal. Calorim. 136 (4) (May 2019) 1817–1830, https://doi.org/10.1007/s10973-018-7809-3.
[23] S. Bhattacharyya, A. Garai, J. Sarkar, Thermodynamic analysis and optimization of a novel N2O–CO2 cascade system for refrigeration and heating, Int. J. Refrig. 32 (5) (Aug. 2009) 1077–1084, https://doi.org/10.1016/j.ijrefrig.2008.09.008.
[24] H.M. Getu, P.K. Bansal, Thermodynamic analysis of an R744–R717 cascade refrigeration system, Int. J. Refrig. 31 (1) (Jan. 2008) 45–54, https://doi.org/10.1016/j.ijrefrig.2007.06.014.
[25] C. Aktemur, I.T. Ozturk, C. Cimsit, Comparative energy and exergy analysis of a subcritical cascade refrigeration system using low global warming potential refrigerants, Appl. Therm. Eng. 184 (Feb. 2021) 116254, https://doi.org/10.1016/j.applthermaleng.2020.116254.
[26] A. Kilicarslan, M. Hosoz, Energy and irreversibility analysis of a cascade refrigeration system for various refrigerant couples, Energy Convers. Manag. 51 (12) (Dec. 2010) 2947–2954, https://doi.org/10.1016/j.enconman.2010.06.037.
[27] R. Llopis, D. Sánchez, C. Sanz-Kock, R. Cabello, E. Torrella, Energy and environmental comparison of two-stage solutions for commercial refrigeration at low temperature: fluids and systems, Appl. Energy 138 (Jan. 2015) 133–142, https://doi.org/10.1016/j.apenergy.2014.10.069.
[28] S. Soni, P. Mishra, G. Maheshwari, D.S. Verma, Theoretical energy analysis of Cascade refrigeration system using low Global warming potential refrigerants, Mater. Today Proc. 63 (2022) 164–169, https://doi.org/10.1016/j.matpr.2022.02.436.
[29] G. Eggen, K. Aflekt, Commercial refrigeration with ammonia and CO2 as working fluids, in: Proceedings of the Third IIR: Gustav Lorentzen Conference on Natural Working Fluids, Oslo, Norway, 1998, pp. 281–292 [Online]. Available: https://iifiir.org/en/fridoc/commercial-refrigeration-with-ammonia-and-co2-as-working-fluids-17112.
[30] A. Pearson, P. Cable, A distribution warehouse with CO2 as refrigerant, in: Proceedings of the International Congress of Refrigeration, Washington, DC, USA, 2003.
[31] V. Riessen, G. J., NH3/CO2 supermarket refrigeration system with CO2 in the cooling and freezing section: technical, energetic and economical issues, in: TNO Environment, Energy and Process Innovation, Apeldoorn, Netherlands, 2004.
[32] S. Sawalha, Carbon Dioxide in Supermarket Refrigeration, KTH, Applied Thermodynamics and Refrigeration, 2008.
[33] A. da Silva, E.P. Bandarra Filho, A.H.P. Antunes, Comparison of a R744 cascade refrigeration system with R404A and R22 conventional systems for supermarkets, Appl. Therm. Eng. 41 (Aug. 2012) 30–35, https://doi.org/10.1016/j.applthermaleng.2011.12.019.
[34] Z. Liu, M. Bai, H. Tan, Y. Ling, Z. Cao, Experimental test on the performance of a −80 °C cascade refrigeration unit using refrigerants R290-R170 for COVID-19 vaccines storage, J. Build. Eng. 63 (Jan. 2023) 105537, https://doi.org/10.1016/j.jobe.2022.105537.
[35] R. Cabello, D. Sánchez, R. Llopis, J. Catalán, L. Nebot-Andrés, E. Torrella, Energy evaluation of R152a as drop in replacement for R134a in cascade refrigeration plants, Appl. Therm. Eng. 110 (Jan. 2017) 972–984, https://doi.org/10.1016/j.applthermaleng.2016.09.010.
[36] W. Bingming, W. Huagen, L. Jianfeng, X. Ziwen, Experimental investigation on the performance of NH3/CO2 cascade refrigeration system with twin-screw compressor, Int. J. Refrig. 32 (6) (Sep. 2009) 1358–1365, https://doi.org/10.1016/j.ijrefrig.2009.03.008.
[37] J.A. Dopazo, J. Fernández-Seara, Experimental evaluation of a cascade refrigeration system prototype with CO2 and NH3 for freezing process applications, Int. J. Refrig. 34 (1) (Jan. 2011) 257–267, https://doi.org/10.1016/j.ijrefrig.2010.07.010.
[38] C. Sanz-Kock, R. Llopis, D. Sánchez, R. Cabello, E. Torrella, Experimental evaluation of a R134a/CO 2 cascade refrigeration plant, Appl. Therm. Eng. 73 (1) (Dec. 2014) 41–50, https://doi.org/10.1016/j.applthermaleng.2014.07.041.
[39] H. Wang, Y. Song, F. Cao, Experimental investigation on the pull-down performance of a -80°C ultra-low temperature freezer, Int. J. Refrig. 119 (Nov. 2020) 1–10, https://doi.org/10.1016/j.ijrefrig.2020.04.030.
[40] M.-J. Jeon, Experimental analysis of the r744/r404a cascade refrigeration system with internal heat exchanger. Part 1: coefficient of performance characteristics, Energies 14 (18) (Sep. 2021) 6003, https://doi.org/10.3390/en14186003.
[41] M. Walid Faruque, M. Hafiz Nabil, M. Raihan Uddin, M. Monjurul Ehsan, S. Salehin, Thermodynamic assessment of a triple cascade refrigeration system utilizing hydrocarbon refrigerants for ultra-low temperature applications, Energy Convers. Manag. X 14 (May 2022) 100207, https://doi.org/10.1016/j.ecmx.2022.100207.
[42] N.B. Najibullah Khan, A. Barifcani, M. Tade, V. Pareek, A case study: application of energy and exergy analysis for enhancing the process efficiency of a three stage propane pre-cooling cycle of the cascade LNG process, J. Nat. Gas Sci. Eng. 29 (Feb. 2016) 125–133, https://doi.org/10.1016/j.jngse.2015.12.034.
[43] J.-I. Yoon, W.-J. Choi, S. Lee, K. Choe, G.-J. Shim, Efficiency of cascade refrigeration cycle using C 3 H 8 , N 2 O, and N 2, Heat Tran. Eng. 34 (11–12) (Sep. 2013) 959–965, https://doi.org/10.1080/01457632.2012.753575.
[44] N. Johnson, J. Baltrusaitis, W.L. Luyben, Design and control of a cryogenic multi-stage compression refrigeration process, Chem. Eng. Res. Des. 121 (May 2017) 360–367, https://doi.org/10.1016/j.cherd.2017.03.018.
[45] Y. Qin, N. Li, H. Zhang, B. Liu, Energy and exergy performance evaluation of a three-stage auto-cascade refrigeration system using low-GWP alternative refrigerants, Int. J. Refrig. 126 (Jun. 2021) 66–75, https://doi.org/10.1016/j.ijrefrig.2021.01.028.
[46] S. Sanaye, A. Shirazi, Thermo-economic optimization of an ice thermal energy storage system for air-conditioning applications, Energy Build. 60 (May 2013) 100–109, https://doi.org/10.1016/j.enbuild.2012.12.040.
[47] V. Jain, G. Sachdeva, S.S. Kachhwaha, NLP model based thermoeconomic optimization of vapor compression–absorption cascaded refrigeration system, Energy Convers. Manag. 93 (Mar. 2015) 49–62, https://doi.org/10.1016/j.enconman.2014.12.095.
[48] R.S. Mitishita, E.M. Barreira, C.O.R. Negrão, C.J.L. Hermes, Thermoeconomic design and optimization of frost-free refrigerators, Appl. Therm. Eng. 50 (1) (Jan. 2013) 1376–1385, https://doi.org/10.1016/j.applthermaleng.2012.06.024.
[49] M.J. Mayer, A. Szilágyi, G. Gróf, Environmental and economic multi-objective optimization of a household level hybrid renewable energy system by genetic algorithm, Appl. Energy 269 (Jul. 2020) 115058, https://doi.org/10.1016/j.apenergy.2020.115058.
[50] S. Karasu, A. Altan, S. Bekiros, W. Ahmad, A new forecasting model with wrapper-based feature selection approach using multi-objective optimization technique for chaotic crude oil time series, Energy 212 (Dec. 2020) 118750, https://doi.org/10.1016/j.energy.2020.118750.

[51] A. Hasani, H. Mokhtari, M. Fattahi, A multi-objective optimization approach for green and resilient supply chain network design: a real-life case study, J. Clean. Prod. 278 (Jan. 2021) 123199, https://doi.org/10.1016/j.jclepro.2020.123199.
[52] P. Cui, M. Yu, Z. Liu, Z. Zhu, S. Yang, Energy, exergy, and economic (3E) analyses and multi-objective optimization of a cascade absorption refrigeration system for low-grade waste heat recovery, Energy Convers. Manag. 184 (Mar. 2019) 249–261, https://doi.org/10.1016/j.enconman.2019.01.047.
[53] B.H. Gebreslassie, E.A. Groll, S.V. Garimella, Multi-objective optimization of sustainable single-effect water/Lithium Bromide absorption cycle, Renew. Energy 46 (Oct. 2012) 100–110, https://doi.org/10.1016/j.renene.2012.03.023.
[54] S. Sanaye, A. Shirazi, Four E analysis and multi-objective optimization of an ice thermal energy storage for air-conditioning applications, Int. J. Refrig. 36 (3) (May 2013) 828–841, https://doi.org/10.1016/j.ijrefrig.2012.10.014.
[55] M. Navidbakhsh, A. Shirazi, S. Sanaye, Four E analysis and multi-objective optimization of an ice storage system incorporating PCM as the partial cold storage for air-conditioning applications, Appl. Therm. Eng. 58 (1–2) (Sep. 2013) 30–41, https://doi.org/10.1016/j.applthermaleng.2013.04.002.
[56] V.K. Patel, B.D. Raja, P. Prajapati, L. Parmar, H. Jouhara, An investigation to identify the performance of cascade refrigeration system by adopting high-temperature circuit refrigerant R1233zd(E) over R161, International Journal of Thermofluids 17 (Feb. 2023) 100297, https://doi.org/10.1016/j.ijft.2023.100297.
[57] R. Roy, B.K. Mandal, Thermo-economic analysis and multi-objective optimization of vapour cascade refrigeration system using different refrigerant combinations, J. Therm. Anal. Calorim. 139 (5) (Mar. 2020) 3247–3261, https://doi.org/10.1007/s10973-019-08710-x.
[58] M. Aminyavari, B. Najafi, A. Shirazi, F. Rinaldi, Exergetic, economic and environmental (3E) analyses, and multi-objective optimization of a CO2/NH3 cascade refrigeration system, Appl. Therm. Eng. 65 (1–2) (Apr. 2014) 42–50, https://doi.org/10.1016/j.applthermaleng.2013.12.075.
[59] S. Eini, H. Shahhosseini, N. Delgarm, M. Lee, A. Bahadori, Multi-objective optimization of a cascade refrigeration system: exergetic, economic, environmental, and inherent safety analysis, Appl. Therm. Eng. 107 (Aug. 2016) 804–817, https://doi.org/10.1016/j.applthermaleng.2016.07.013.
[60] K.K. Singh, R. Kumar, A. Gupta, Multi-objective optimization of thermodynamic and economic performances of natural refrigerants for cascade refrigeration, Arabian J. Sci. Eng. 46 (12) (Dec. 2021) 12235–12252, https://doi.org/10.1007/s13369-021-05924-w.
[61] S. Sholahudin Nasruddin, N. Giannetti, Arnas, "Optimization of a cascade refrigeration system using refrigerant C3H8 in high temperature circuits (HTC) and a mixture of C2H6/CO2 in low temperature circuits (LTC),", Appl. Therm. Eng. 104 (Jul. 2016) 96–103, https://doi.org/10.1016/j.applthermaleng.2016.05.059.
[62] E. Gholamian, P. Hanafizadeh, P. Ahmadi, Advanced exergy analysis of a carbon dioxide ammonia cascade refrigeration system, Appl. Therm. Eng. 137 (Jun. 2018) 689–699, https://doi.org/10.1016/j.applthermaleng.2018.03.055.
[63] F. Yilmaz, R. Selbaş, Comparative thermodynamic performance analysis of a cascade system for cooling and heating applications, Int. J. Green Energy 16 (9) (Jul. 2019) 674–686, https://doi.org/10.1080/15435075.2019.1618308.
[64] T. Morosuk, G. Tsatsaronis, Splitting physical exergy: theory and application, Energy 167 (2019) 698–707, https://doi.org/10.1016/j.energy.2018.10.090.
[65] T. Morosuk, G. Tsatsaronis, Advanced exergetic evaluation of refrigeration machines using different working fluids, Energy 34 (12) (Dec. 2009) 2248–2258, https://doi.org/10.1016/j.energy.2009.01.006.
[66] M. Deymi-Dashtebayaz, A. Sulin, T. Ryabova, I. Sankina, M. Farahnak, R. Nazeri, Energy, exergoeconomic and environmental optimization of a cascade refrigeration system using different low GWP refrigerants, J. Environ. Chem. Eng. 9 (6) (2021) 106473, https://doi.org/10.1016/j.jece.2021.106473.
[67] A.H. Mosaffa, L.G. Farshi, C.A. Infante Ferreira, M.A. Rosen, Exergoeconomic and environmental analyses of CO2/NH3 cascade refrigeration systems equipped with different types of flash tank intercoolers, Energy Convers. Manag. 117 (Jun. 2016) 442–453, https://doi.org/10.1016/j.enconman.2016.03.053.
[68] J. Wang, Z. John Zhai, Y. Jing, C. Zhang, Particle swarm optimization for redundant building cooling heating and power system, Appl. Energy 87 (12) (Dec. 2010) 3668–3679, https://doi.org/10.1016/j.apenergy.2010.06.021.
[69] M.H. Nabil, Y. Khan, M.W. Faruque, M.M. Ehsan, Thermo-economic assessment of advanced triple cascade refrigeration system incorporating a flash tank and suction line heat exchanger, Energy Convers. Manag. 295 (Nov. 2023) 117630, https://doi.org/10.1016/j.enconman.2023.117630.
[70] Q. Wang, et al., Comparative Analysis of Thermodynamic Performance of Three-Stage Cascade Refrigeration System Assisted with Internal Heat Exchanger, 2020.
[71] G.-Y. Ma, H.-X. Zhao, Experimental study of a heat pump system with flash-tank coupled with scroll compressor, Energy Build. 40 (5) (Jan. 2008) 697–701, https://doi.org/10.1016/j.enbuild.2007.05.003.
[72] E.H. Houssein, M.A. Mahdy, D. Shebl, A. Manzoor, R. Sarkar, W.M. Mohamed, An efficient slime mould algorithm for solving multi-objective optimization problems, Expert Syst. Appl. 187 (Jan. 2022) 115870, https://doi.org/10.1016/j.eswa.2021.115870.
[73] B. Abdollahzadeh, F.S. Gharehchopogh, A multi-objective optimization algorithm for feature selection problems, Eng. Comput. 38 (S3) (Aug. 2022) 1845–1863, https://doi.org/10.1007/s00366-021-01369-9.
[74] N. Zhang, P. Bénard, R. Chahine, T. Yang, J. Xiao, Optimization of pressure swing adsorption for hydrogen purification based on Box-Behnken design method, Int. J. Hydrogen Energy 46 (7) (Jan. 2021) 5403–5417, https://doi.org/10.1016/j.ijhydene.2020.11.045.
[75] S. Shengli, L. Junping, L. Qi, N. Fangru, F. Jia, X. Shulian, Optimized preparation of Phragmites australis activated carbon using the Box-Behnken method and desirability function to remove hydroquinone, Ecotoxicol. Environ. Saf. 165 (June) (2018) 411–422, https://doi.org/10.1016/j.ecoenv.2018.09.038.
[76] A. Konak, D.W. Coit, A.E. Smith, Multi-objective optimization using genetic algorithms: a tutorial, Reliab. Eng. Syst. Saf. 91 (9) (Sep. 2006) 992–1007, https://doi.org/10.1016/j.ress.2005.11.018.
[77] S. Diyaley, P. Shilal, I. Shivakoti, R.K. Ghadai, K. Kalita, PSI and TOPSIS based selection of process parameters in WEDM, Period. Polytech. - Mech. Eng. 61 (4) (Sep. 2017) 255, https://doi.org/10.3311/PPme.10431.
[78] H.R. Shahhosseini, M. Farsi, S. Eini, Multi-objective optimization of industrial membrane SMR to produce syngas for Fischer-Tropsch production using NSGA-II and decision makings, J. Nat. Gas Sci. Eng. 32 (May 2016) 222–238, https://doi.org/10.1016/j.jngse.2016.04.005.
[79] F. Musharavati, S. Khanmohammadi, A. Pakseresht, S. Khanmohammadi, Waste heat recovery in an intercooled gas turbine system: exergo-economic analysis, triple objective optimization, and optimum state selection, J. Clean. Prod. 279 (Jan. 2021) 123428, https://doi.org/10.1016/j.jclepro.2020.123428.